ABSTRACT

Park, Man Sik. Symmetry and Separability In Spatial-Temporal Processes. (Under the direction of Dr. Montserrat Fuentes.)

Symmetry is one of most standard assumptions that are needed for a covariance function in spatial statistics. However, many studies in spatial research fields show that environmental data have complex spatial-temporal dependency structures that are difficult to model and estimate, due to the lack of symmetry and other standard assumptions of a covariance function. So, not much literature exists in statistics about asymmetric covariance functions and formal tests for lack of symmetry in spatial-temporal processes. In this study, we introduce certain types of symmetry in spatial-temporal processes and propose new classes of asymmetric spatial-temporal covariance models by using spectral representations. We also clarify the relationship between symmetry and separability and introduce nonseparable covariance models. Based on the proposed concept of symmetry in spatial-temporal processes, new formal tests for lack of symmetry are proposed in this study by employing spectral representations of the spatial-temporal covariance function. The advantage of the tests is that simple analysis of variance (ANOVA) approaches are employed for detecting lack of symmetry inherent in spatial-temporal processes. Our new classes of covariance models are applied to the methods for the fine particulate matters with a mass median diameter less than 2.5 μm ($PM_{2.5}$) observed from U.S. Environmental Protection Agency (EPA). We evaluate the performance of the tests by a simulation study and, finally, apply to

the $PM_{2.5}$ daily concentration calculated by the Models-3/Community Multiscale Air Quality (CMAQ) modeling system with the spatial resolution of $36km \times 36km$.

Symmetry and Separability In Spatial-Temporal Processes

by

Man Sik Park

A dissertation submitted to the Graduate Faculty of
North Carolina State University
in partial fulfillment of the
requirements for the Degree of
Doctor of Philosophy

STATISTICS

Raleigh

2005

APPROVED BY:

Dr. Montserrat Fuentes Chair of Advisory Committee	Dr. Peter Bloomfield
Dr. David A. Dickey	Dr. Sastry G. Pantula
Dr. Jerry M. Davis	

To my family

Biography

Man Sik Park was born in Youngdong, Republic of Korea on October 1, 1972. He entered the Department of Statistics at Korea University in 1991 and earned his B.S. in 1998 and M.S. in 2000 in mathematical statistics. He joined the department of Statistics, North Carolina State University for the pursuit of Ph.D. degree. He has been accepted as a post-doctoral research position in the department of Statistics at Colorado State University.

Acknowledgements

I would like to thank the members of my advisory committee for their advice and support during the preparation of my dissertation.

I am extremely grateful for having Dr.Montserrat Fuentes as my advisor. Her enthusiasm, knowledgeable guidance, and constant support, including financial support, have meant a tremendous amount to me. She is not only an excellent researcher who imposes the highest standards on her academic work, but also an outstanding advisor who provides continuing encouragement for her students. I thank her for her encouragement to become an independent researcher, and I also admire tireless energy and her devotion to her professional career.

Thanks to Dr. Peter Bloomfield for his valuable comments and suggestions on spectral analysis approaches. Thanks to Dr. Dave A. Dickey for his advice and encouragement during my work on my dissertation. Thanks to Dr. Sastry G. Pantula for his helpful questions and suggestions that have helped me to present the material much better. I also would like to thank Dr. William H. Swallow and all my professors, Terry Byron, and Adrian Blue for all their help and encouragement over these past 3 years. I am also grateful to Dr. David M. Holland, my collaborator, working at EPA for his insightful comments about the real applications.

Finally I would like to express my deepest gratitude and biggest appreciation to my parents. I also would like to thank my wife, Eunnam, and my son, Robin, for their unceasing support and endless love.

Contents

List of Tables

List of Figures

Chapter 1

Introduction

The most common problem that researchers in diverse fields such as epidemiology, ecology, climatology, and environmental health research are confronted with is how to predict the observations at unobserved sites using the given data. To do that, they estimate the underlying parameters in certain covariance structures that are assumed to explain the given data very well. Most data are observed in space and time. Both spatial and temporal effects are considered for the spatial interpolation and the temporal forecast.

In general, the spatial-temporal processes have a much more complicated structure than spatial process alone. Since spatial structure and temporal structure are entangled in the covariance structure, it is not easy to model these two parts simultaneously. In order to overcome the difficulty in modelling the spatial-temporal covariance structure, the concept of "separability" has been applied. A spatial-temporal process is separable if the spatial-temporal covariance structure can be

divided into a spatial covariance and temporal covariance, separately. Separable spatial-temporal classes give us many advantages, such as the simplified representation of the covariance matrix and, consequently, important computational benefits. But in real applications, it may not be reasonable to estimate the covariances that depend on space and time separately and combine them together for predicting observations at unobserved sites or times. Many reseachers (Cressie and Huang (1999), Gneiting (2002) and so on) have proposed nonseparable covariance classes for spatial-temporal processes. Recently Fuentes *et al.* (2005) introduced a new nonseparable class with a unique parameter reflecting the dependency between the spatial and temporal components.

"Isotropy" is also one of the common problems that the researchers should take into account when analyzing data. A spatial process is isotropic if the covariance between any two arbitrary sites only depends on the distance no matter what the relative position between them is. As you can see from Figure 1.1, under the isotropic condition, the covariance between $\mathbf{a}$ and $\mathbf{b}$ is the same as the covariance between $\mathbf{a}$ and $\mathbf{b}'$ because of the same distance, r_1. So, the isotropic covariance in two-dimensional space does not depend on any direction. This condition, however, is too unrealistic to apply to real conditions. We can enumerate many examples that do not satisfy the isotropic condition. The dispersion of air pollutants from a chemical factory is directly affected by the wind speed as well as wind direction. The patterns of annual temperature in United States can be somehow divided by some geographic information such as longitude and latitude.

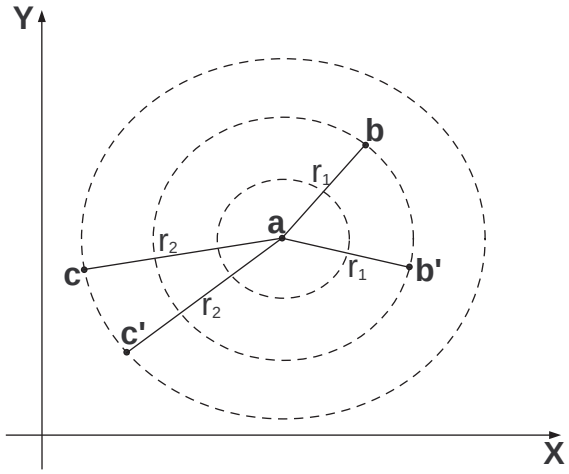

Figure 1.1: Isotropy in Two-Dimensional Space

So "anisotropy" should be considered. Anisotropic covariance depends not only on distance between sites but also on their relative orientation. As one can see from Figure 1.2, the covariance between **a** and **b** is different from the covariance between **a** and $\mathbf{b}'$ despite separation by the same distance, r_1. In order to check the existence of certain types of anisotropy, we make use of a "rose diagram" or a "directional semivariogram". Then, we transform the covariance structure to achieve isotropy. Geometric anisotropy is the simplest case. We can make the covariance structure satisfy isotropy by estimating the parameters for strength and rotation. Zimmerman (1993) proposes three different kinds of nongeometric anisotropy: 1) sill anisotropy; 2) nugget anisotropy; and 3) range anisotropy. Figure 2 shows another important infomation that has not been considered so far. Under geometric anisotropy we find that the covariance between **a** and $\mathbf{b}^*$ separated by distance r_1 is the same as the covariance between **a** and $\mathbf{b}'$. The two lines

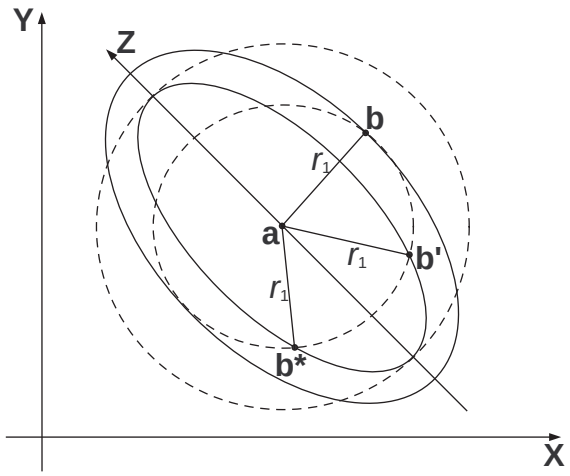

Figure 1.2: Geometric Anisotropy in Two-Dimensional Space

between **a** and $\mathbf{b}^*$ and between **a** and $\mathbf{b}'$ are symmetric with respect to Z-axis. So anisotropy may present some patterns of spatial or spatial-temporal dependency, which can be specified by "symmetry". A few researchers have dealt with symmetry in the environmental field. Scaccia and Martin (2005) introduced certain types of symmetry in the spatial processes: 1) axial symmetry; 2) diagonal symmetry; and 3) complete symmetry, and proposed some tests for symmetry using spectral methods. Their work, however, focuses on only two dimensional spatial process ignoring time effect, and is applied to a complete regular lattice structure. In spatial-temporal processes there can be four different types of symmetry in spatial-temporal processes: 1) axial symmetry in time; 2) axial symmetry in space; 3) diagonal symmetry in time; and 4) diagonal symmetry in space.

Symmetry also has the same advantages as separability does. Symmetry can

provide some advantages to help researchers construct simplified covariance structures for spatial-temporal processes, and to make better interpretations of the underlying characteristics of the processes. The differences between separability and symmetry, however, are apparent. Separability only takes into account temporal lag and spatial separation, which consists of the product of two covariance functions. Symmetry, however, takes into account each spatial lag as well as temporal lag. So, in spatial-temporal processes, separability does not always guarantee symmetry. Since it is difficult to statistically determine isotropy in spatial-temporal processes, symmetry can play an important role as its substitute.

In this study, we characterize the aforementioned types of symmetry in spatial-temporal processes, and develop a new testing method for each case of symmetry with asymptotic properties of cross-spectral density function and coherency. Finally, we develop a new class of nonsymmetric spatial-temporal stationary covariance models.

This study is organized as follows. In chapter 2, we introduce new concepts of symmetry inherent to spatial-temporal processes, develop a new class of asymmetric spatial-temporal stationary covariance models, and apply our new class to the real application. In chapter 3, we propose new formal tests for lack of symmetry by employing the spectral representations of spatial-temporal covariance function and validate the tests with the simulation study and the the application to air-pollution datasets. Chapter 4 focuses on the conclusion and the further research of this study.

Chapter 2

New Classes of Asymmetric Spatial-Temporal Covariance Models

2.1 Introduction

Many studies in diverse fields such as climatology, ecology, and public health research show that environmental data have complex spatial-temporal dependency structures that are difficult to model and estimate. In general, the spatial-temporal processes have more complicated structures than the spatial processes alone. The main reason is that, since the spatial and the temporal structure are entangled in the covariance function, it is not easy to take into account these two structures simultaneously. In order to overcome the difficulty in building the spatial-temporal processes, we usually employ two major concepts in spatial-

temporal processes: separability and symmetry.

Separability in spatial-temporal processes enables us to easily construct the model due to advantages such as the simplified representation of the covariance matrix, consequently, remarkable computational benefit. Suppose that $\{Z(\mathbf{s},t) : \mathbf{s} \in D \subset \mathbb{R}^d,\ t \in [0,\infty)\}$ denote a stationary spatial-temporal process measured at N sites and T times, and the covariance function is defined as

$$C(\mathbf{s}_i - \mathbf{s}_j; t_k - t_l|\boldsymbol{\theta}) \equiv \text{cov}\{Z(\mathbf{s}_i, t_k), Z(\mathbf{s}_j, t_l)\}; \quad \mathbf{s}_i, \mathbf{s}_j \in D, \quad t_k, t_l \in [0,\infty), \tag{2.1}$$

where $\mathbf{s}_i = (s_1^i, \cdots, s_d^i)'$ and C satisfies the positive definiteness for all $\boldsymbol{\theta} \in \boldsymbol{\Theta} \subset \mathbb{R}^p$. Then the process is called separable if the covariance function in (2.1) can be divided into a spatial covariance and temporal covariance, that is,

$$C(\mathbf{s}_i - \mathbf{s}_j; t_k - t_l|\boldsymbol{\theta}) = C_{\mathbf{s}}(\mathbf{s}_i - \mathbf{s}_j|\boldsymbol{\theta}_{\mathbf{s}}) \cdot C_T(t_k - t_l|\boldsymbol{\theta}_t), \tag{2.2}$$

where $C_{\mathbf{s}}$ is a positive definite spatial covariance function in $\mathbb{R}^d$, C_T is a positive definite temporal covariance function in $\mathbb{R}^1$, and $\boldsymbol{\theta} = (\boldsymbol{\theta}_{\mathbf{s}}', \boldsymbol{\theta}_t')'$. Under stationarity condition, (2.2) is rewritten as

$$C(\mathbf{h}; u|\boldsymbol{\theta}) = C_{\mathbf{s}}(\mathbf{h}|\boldsymbol{\theta}_{\mathbf{s}}) \cdot C_T(u|\boldsymbol{\theta}_t), \tag{2.3}$$

for all $\mathbf{h} \equiv (h_1, \cdots, h_d)' = \mathbf{s}_i - \mathbf{s}_j$ is a vector of spatial lags and all $u = t_k - t_l$ is a temporal lag (see Rodriguez-Iturbe and Majia (1974)). However, in real applications, it may not be reasonable to estimate the covariance functions that depend on space and time separately, and then, combine them together for predicting observations at unobserved sites or times. Especially, in air pollution data it is

not easy to capture the underlying pattern just by relying on separability. Many reseachers have proposed nonseparable covariance classes for spatial-temporal processes. Jones and Zhang (1997) develop a parametric family of spectral density functions, with corresponding nonseparable stationary covariance functions, by adapting stochastic partial differential equations. Cressie and Huang (1999) introduce new classes of nonseparable, spatial-temporal stationary covariance functions with space-time interaction. The separable covariance function is a special case. Their main idea is to develop the nonseparable positive-definite covariance function with spatial-temporal interaction by specifying two appropriate functions each of which is expressed as a spectral representation in closed form. Gneiting (2002) proposes general classes of nonseparable, stationary spatial-temporal covariance functions which are directly constructed in the space-time domain and are based on Fourier-free implementation. This paper insists that any spatial-temporal covariance function can be modeled without the Fourier transformation as long as one finds appropriate functions. Recently Fuentes *et al.* (2005) introduce a new class of nonseparable covariance models with a unique parameter reflecting the dependency between the spatial and the temporal components. Instead of a covariance function which is the multiplication of spatial and temporal covariances (see (2.3)), Myers and Journel (1990), and Rouhani and Myers (1990) consider the separability under which the covariance function is the addition of spatial and temporal covariances (see (2.2)), although the covariance matrix turns out to be singular in some situations.

The other concept for relieving the difficulty in modeling is symmetry. Symmetry also has the same advantages as separability does. Symmetry plays an important role in helping researchers construct simplified covariance structures for spatial-temporal processes, and making better interpretations of the underlying characteristics of the processes. Due to these benefits symmetry has been assumed and even, has been taken for granted. In these days, more attention has been focused on lack of symmetry although only a few studies have been accomplished so far. One of the noteworthy studies is Scaccia and Martin (2005), which, for a spatial process, $\{Z(\mathbf{s}) : \mathbf{s} \in D \subset \mathbb{R}^d\}$, especially for two-dimensional spatial lattice data, introduce two types of symmetry (axial symmetry; diagonal symmetry) and separability which are, respectively, denoted by, for all h_1 and h_2

$$C(h_1, h_2) = C(-h_1, h_2), \tag{2.4}$$

$$C(h_1, h_2) = C(h_2, h_1), \tag{2.5}$$

and

$$C(h_1, h_2) = C_1(h_1) \cdot C_2(h_2), \tag{2.6}$$

where $C(h_1, h_2) \equiv \text{cov}(Z(s_1 + h_1, s_2 + h_2), Z(s_1, s_2))$, and C_1 and C_2 are the positive-definite covariances of first and second spatial lag. They also develop new tests for axial symmetry in (2.4) and separability in (2.6) based on periodograms. Using certain ratios of spatial periodograms, Lu and Zimmerman (2005) propose new diagnostic tests for axial symmetry and complete symmetry which means that (2.4) and (2.5) are both satisfied. However, there has been no

trial for adapting symmetry to the general spatial-temporal setting except Stein (2005), which proposes spatial-temporal covariance models with lack of axial symmetry in time presented in Section 2.2. The approach in this study is based on generating asymmetric models from symmetric ones by taking derivatives. In this study we introduce certain types of symmetry in spatial-temporal processes, and propose new classes of nonseparable spatial-temporal covariance models with spatial-temporal dependency parameters. These classes are directly derived from a simple and valid spectral density function and, hence, are represented in closed form.

This chapter is organized as follows. In Section 2.2, we define three types of symmetry realized in the spatial-temporal setting. Based on the definition of symmetry we develop new classes of nonseparable covariance models in Section 2.3. In Section 2.4, we clarify the relationship between symmetry and separability and extend the proposed models to the nonseparable case. In Section 2.5, the proposed covariance models will be fitted to spatial-temporal data on Particulate Matter with a mass median diameter less than 2.5 μm ($PM_{2.5}$) over the northeastern region of U.S. Finally, we briefly discuss our approach in Section 2.6.

2.2 Symmetry in Spatial-Temporal Processes

In this section, we define three types of symmetry in spatial-temporal processes; axial symmetry in time, axial symmetry in space, and diagonal symmetry

in space. In this article we assume that any covariance function is stationary in time unless otherwise mentioned. The first type of symmetry is axial symmetry in time.

Definition 2.2.1 *A process is called axially symmetric in time if for any temporal lag* $u \neq 0$*,*

$$C(\mathbf{s}_i - \mathbf{s}_j; u) = C(\mathbf{s}_{i^*} - \mathbf{s}_{j^*}; -u), \tag{2.7}$$

for arbitrary four locations (i, j, i^*, j^*) *satisfying* $\mathbf{s}_i - \mathbf{s}_j = \mathbf{s}_{i^*} - \mathbf{s}_{j^*}$*.*

Under stationarity in space, (2.7) is reduced to

$$C(\mathbf{h}; u) = C(\mathbf{h}; -u), \tag{2.8}$$

where $\mathbf{s}_i = \mathbf{s}_j + \mathbf{h}$ and $\mathbf{s}_{i^*} = \mathbf{s}_{j^*} + \mathbf{h}$. What is important here is that the directions and the distances on spatial domain are the same, and the temporal lags have the same magnitudes but different signs. The second type of symmetry is axial symmetry in space.

Definition 2.2.2 *A process is called axially symmetric in space if*

$$C(\mathbf{h}; u) = C(\mathring{\mathbf{h}}; u), \tag{2.9}$$

where $\mathring{\mathbf{h}} = (h_1, \cdots, h_{k-1}, -h_k, h_{k+1}, \cdots, h_d)'$ *for* k *fixed.*

As can be seen in (2.9), for temporal lag u fixed, all the spatial lags are the same except one spatial lag, which has different sign. The process can be also called (k)-axially symmetric in space. $\mathring{\mathbf{h}} = (h_1, -h_2)'$ is one possible case in case of $d = 2$. The last one is diagonal symmetry in space.

Definition 2.2.3 *A process is called (k-l) diagonally symmetric in space if*

$$C(\mathbf{h}; u) = C(\ddot{\mathbf{h}}; u), \tag{2.10}$$

where $\ddot{\mathbf{h}} = (h_1, \cdots, h_{k-1}, h_l, h_{k+1}, \cdots, h_{l-1}, h_k, h_{l+1}, \cdots, h_d)'$ *for* $k \neq l$.

From (2.10) we can see that only two spatial lags, h_k and h_l, are switched with each other. Provided that $d = 2$, $\ddot{\mathbf{h}} = (h_2, h_1)'$.

2.3 Classes of Asymmetric Stationary Covariance Models

We defined three different types of symmetry in spatial-temporal processes in Section 2.2. Now we propose new classes of asymmetric spatial-temporal stationary covariance models. In this section, we provide a new and simple method to construct such covariance models. The main idea of our approach is to build covariance functions directly derived from the corresponding spectral density functions. In order to do that, we propose the spatial-temporal spectral density function given by

$$\begin{aligned} f_{\mathbf{v}}(\boldsymbol{\omega}; \tau) &= \gamma \left(\alpha^2\beta^2 + \beta^2 \|\boldsymbol{\omega} + \tau \mathbf{v}_1\|^2 + \alpha^2(\tau + \mathbf{v}_2'\boldsymbol{\omega})^2 \right)^{-\nu} \\ &= f_0(\boldsymbol{\omega} + \tau\mathbf{v}_1; \tau + \mathbf{v}_2'\boldsymbol{\omega}), \end{aligned} \tag{2.11}$$

where $f_0(\boldsymbol{\omega}; \tau) \equiv \gamma(\alpha^2\beta^2 + \beta^2\|\boldsymbol{\omega}\|^2 + \alpha^2\tau^2)^{-\nu}$ is the spectral density function transformed from an simple stationary spatial-temporal covariance function, γ, α and β are positive, $\nu > \frac{d+1}{2}$, and $|\mathbf{v}_1'\mathbf{v}_2| < 1$. Here $\mathbf{v}_1 = \{v_{1i}\}_{i=1}^d$ and $\mathbf{v}_2 = \{v_{2i}\}_{i=1}^d$ are vectors satisfying certain types of asymmetry. The spectral density function

in (2.11) is always valid and its Fourier transformation always exists because the following two conditions are satisfied:

C.1 $f_{\mathbf{v}}(\boldsymbol{\omega};\tau) > 0$ everywhere

C.2 $f_{\mathbf{v}}(\boldsymbol{\omega};\tau) < \infty$ for all $\mathbf{v}_1,\ \mathbf{v}_2 \in \mathbb{R}^d$ satisfying $|\mathbf{v}_1'\mathbf{v}_2| < 1$.

So, $C_{\mathbf{v}}(\mathbf{h};u) = \int_{\mathbb{R}^d}\int_{\mathbb{R}} \exp\{i\mathbf{h}'\boldsymbol{\omega} + iu\tau\} f_{\mathbf{v}}(\boldsymbol{\omega};\tau)\ d\tau\ d\boldsymbol{\omega}$ exists and has the positive-definiteness. We can write the corresponding covariance function from the spectral density function, $f_{\mathbf{v}}$ in (2.11) as

$$\begin{aligned} C_{\mathbf{v}}(\mathbf{h};u) &= \int_{\mathbb{R}^d}\int_{\mathbb{R}} \exp\{i\mathbf{h}'\boldsymbol{\omega} + iu\tau\} f_0(\boldsymbol{\omega} + \tau\mathbf{v}_1; \tau + \mathbf{v}_2'\boldsymbol{\omega})\ d\tau\ d\boldsymbol{\omega} \\ &= \int_{\mathbb{R}^d}\int_{\mathbb{R}} \exp\left\{ i\frac{(\widetilde{\mathbf{h}} - u\mathbf{v}_2)'}{1-\mathbf{v}_1'\mathbf{v}_2}\boldsymbol{\omega} + i\frac{(u - \mathbf{h}'\mathbf{v}_1)}{1-\mathbf{v}_1'\mathbf{v}_2}\tau \right\} \frac{f_0(\boldsymbol{\omega};\tau)}{1-\mathbf{v}_1'\mathbf{v}_2}\ d\tau\ d\boldsymbol{\omega} \\ &= \frac{1}{1-\mathbf{v}_1'\mathbf{v}_2}\, C_0\left(\frac{\widetilde{\mathbf{h}} - u\mathbf{v}_2}{1-\mathbf{v}_1'\mathbf{v}_2}; \frac{u - \mathbf{h}'\mathbf{v}_1}{1-\mathbf{v}_1'\mathbf{v}_2} \right), \end{aligned} \tag{2.12}$$

where C_0 is a simple stationary spatial-temporal covariance function, and

$$\widetilde{\mathbf{h}} = \left\{\widetilde{h}_i\right\}_{i=1}^d = \left\{ \left(1 - \sum_{j\neq i} v_{1j}v_{2j} \right) h_i + v_{2i} \sum_{j\neq i} v_{1j}h_j \right\}_{i=1}^d .$$

By straightforward derivation with help of Stein (2005), and Gradshteyn and Ryzhik (2000) (see Appendix), we finally obtain the closed form of the $(d+1)$ dimensional Matérn-type covariance function denoted by

$$\begin{aligned} C_{\mathbf{v}}(\mathbf{h};u) =& \frac{1}{1-\mathbf{v}_1'\mathbf{v}_2} \times \frac{\gamma\pi^{(d+1)/2}\alpha^{-2\nu+d}\beta^{-2\nu+1}}{2^{\nu-(d+1)/2-1}\Gamma(\nu)} \\ & \times \mathcal{M}_{\nu-\frac{d+1}{2}}\left(\sqrt{ \left\{ \frac{\alpha\|\widetilde{\mathbf{h}} - u\mathbf{v}_2\|}{1-\mathbf{v}_1'\mathbf{v}_2} \right\}^2 + \left\{ \frac{\beta(u - \mathbf{h}'\mathbf{v}_1)}{1-\mathbf{v}_1'\mathbf{v}_2} \right\}^2 } \right), \end{aligned} \tag{2.13}$$

where $\mathcal{M}_\nu(r) = r^\nu \mathcal{K}_\nu(r)$ and $\|\cdot\|$ denotes the Euclidean distance. Here $\mathcal{K}_\nu$ is a modified Bessel function of the third kind of order ν. Before going further, we explain the characteristics of the covariance parameters. α and β explain the decaying rates of the spatial and the temporal correlations. So their inverses are interpreted as spatial and temporal ranges. ν measures the degree of smoothness, which means that the larger the ν is, the smoother a process is. What is more important here are the asymmetry vectors $\mathbf{v}_1$ and $\mathbf{v}_2$. As one can see in (2.12) and (2.13), $u - \mathbf{h}'\mathbf{v}_1$ is a temporal lag adjusted by a vector of spatial lags and $\widetilde{\mathbf{h}} - u\mathbf{v}_2$ is a vector of spatial lags adjusted by a temporal lag. So, we can see that the units of $\mathbf{v}_1$ are temporal lag divided by spatial lags, which are called the inverse of speeds. We can also know that the units of $\mathbf{v}_2$ are spatial lags over temporal lag, which are called the velocities. In the rest of this section, we regard the space-time domain as three-dimensional space for the better understanding. $\mathbf{v}_1$ and $\mathbf{v}_2$ take part in developing new classes of asymmetric covariance models and yield the covariance models with the following types of symmetry:

T.1 axial symmetry in time if $\mathbf{v}_1 = \mathbf{v}_2 = \mathbf{0}$

T.2 axial symmetry in space if $v_{11} \neq 0$ or $v_{21} \neq 0$ and $v_{12} = v_{22} = 0$

T.3 diagonal symmetry in space if $v_{11} = v_{12} \neq 0$ and $v_{21} = v_{22} \neq 0$

T.4 asymmetry in space and time otherwise.

From the values of $\mathbf{v} = (v_1, v_2)'$ related to certain type of symmetry, we can know that all types of symmetry proposed in this paper are mutually exclusive from the

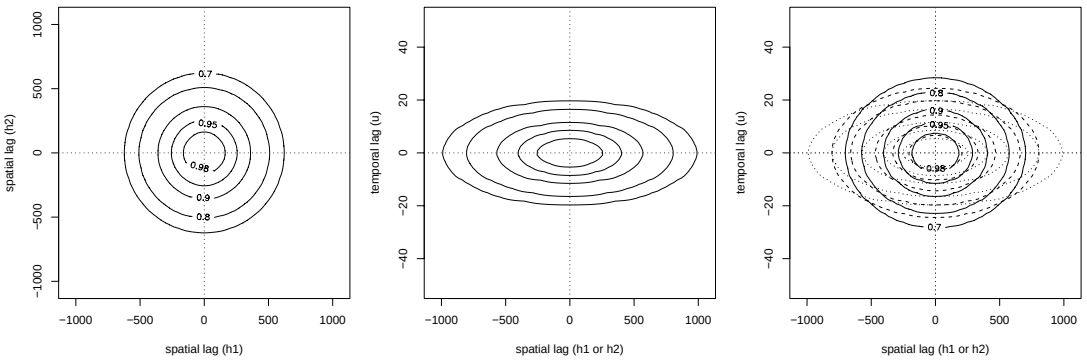

(a) (b) (c)

Figure 2.1: Contour plots for $C(\mathbf{h}; u)$ axially symmetric in time ($\mathbf{v} = \mathbf{0}$), where each number in plot indicates the corresponding percentile of the covariance with $\gamma = 1$, and $\nu = d = 2$. (a) Contour plot of C versus h_1 and h_2 for all u, where $\alpha = 0.02$ and $\beta = 1$; (b) contour plot of C versus h_1 (or h_2) and u, where $\alpha = \sqrt{2}$ and $\beta = 1$; (c) contour plot of C with $\alpha = 0.02, 0.03, 0.04$ and $\beta = 1$. Dotted line is for the first case, solid line for the second, and dashed line for the third.

point of view of $\mathbf{v} = (v_1, v_2)'$ in **T.1**–**T.4**. For the simplification of an asymmetric covariance function in (2.13), we can consider, as special cases, the two covariance models as follow:

$$\begin{aligned} C_{\mathbf{v}_1}(\mathbf{h}; u) =& \frac{\gamma \pi^{(d+1)/2} \alpha^{-2\nu+d} \beta^{-2\nu+1}}{2^{\nu-(d+1)/2-1}\Gamma(\nu)} \left(\alpha \sqrt{\left\{ \frac{\beta(u - \mathbf{h}'\mathbf{v}_1)}{\alpha} \right\}^2 + \|\mathbf{h}\|^2} \right)^{\nu - \frac{d+1}{2}} \\ & \times \mathcal{K}_{\nu - \frac{d+1}{2}} \left(\alpha \sqrt{\left\{ \frac{\beta(u - \mathbf{h}'\mathbf{v}_1)}{\alpha} \right\}^2 + \|\mathbf{h}\|^2} \right), \end{aligned} \tag{2.14}$$

and

$$\begin{aligned} C_{\mathbf{v}_2}(\mathbf{h}; u) =& \frac{\gamma \pi^{(d+1)/2} \alpha^{-2\nu+d} \beta^{-2\nu+1}}{2^{\nu-(d+1)/2-1}\Gamma(\nu)} \left(\alpha \sqrt{\left(\frac{\beta u}{\alpha} \right)^2 + \|\mathbf{h} - u\mathbf{v}_2\|^2} \right)^{\nu - \frac{d+1}{2}} \\ & \times \mathcal{K}_{\nu - \frac{d+1}{2}} \left(\alpha \sqrt{\left(\frac{\beta u}{\alpha} \right)^2 + \|\mathbf{h} - u\mathbf{v}_2\|^2} \right). \end{aligned} \tag{2.15}$$

The corresponding spectral density functions are, respectively, given by

$$\begin{aligned} f_{\mathbf{v}_1}(\boldsymbol{\omega};\tau) &= \gamma\left(\alpha^2\beta^2 + \beta^2\|\boldsymbol{\omega}+\tau\mathbf{v}_1\|^2 + \alpha^2\tau^2\right)^{-\nu} \\ &= f_0(\boldsymbol{\omega}+\tau\mathbf{v}_1;\tau), \end{aligned} \tag{2.16}$$

and

$$\begin{aligned} f_{\mathbf{v}_2}(\boldsymbol{\omega};\tau) &= \gamma\left(\alpha^2\beta^2 + \beta^2\|\boldsymbol{\omega}\|^2 + \alpha^2(\tau+\mathbf{v}_2'\boldsymbol{\omega})^2\right)^{-\nu} \\ &= f_0(\boldsymbol{\omega};\tau+\mathbf{v}_2'\boldsymbol{\omega}). \end{aligned} \tag{2.17}$$

It is certain that both $f_{\mathbf{v}_1}(\boldsymbol{\omega};\tau)$ and $f_{\mathbf{v}_2}(\boldsymbol{\omega};\tau)$ are valid, so the corresponding covariance functions in (2.14) and (2.15) are always positive-definite.

Now we talk about the characteristics of an asymmetric stationary covariance function in (2.14) derived from (2.16). As you can see, $\mathbf{v}_1$ controls the types of symmetry inhereent in spatial-temporal processes. Figure 2.1 displays the behaviors of a spatial-temporal covariance function axially symmetric in time. As one can see, under the axial symmetry in time, the covariance function with the center of the origin always stays whatever $\mathbf{h}$ and u are (Figure 2.1(a),(b)). The decaying rate parameters, α and β only change the shape (Figure 2.1(c)). Figure 2.2 shows that the pattern of a covariance axially symmtric in space depends on temporal lag, u as well as a spatial lag, h_1 not h_2. As one can see, a process with the covariance function moves on the axes of longitudinal lag, h_1 and temporal lag, u, and the direction of movement depends on the signs of u and h_1, respectively (Figure 2.2(a),(c)). From Figure 2.2(b), we know that the the term about temporal effect, $u - \mathbf{h}'\mathbf{v}_1$ does not depend on the latitudinal lag, h_2 because $v_2 = 0$. Figure 2.3 displays the behavior of the covariance function diagonally symmetric in space.

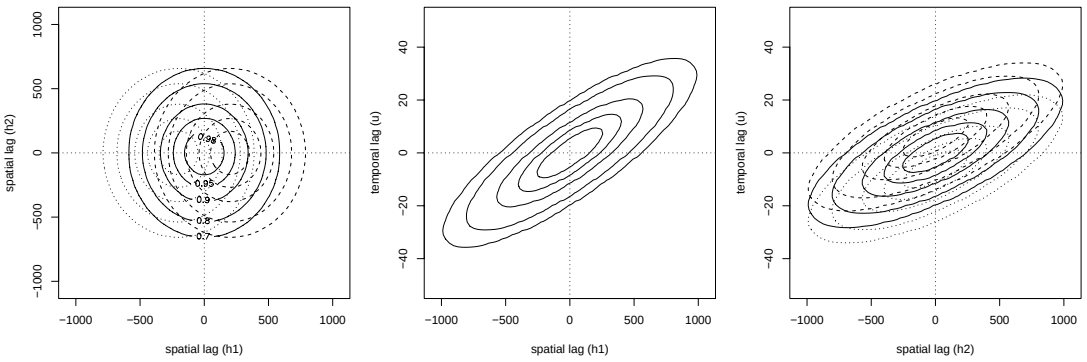

(a) (b) (c)

Figure 2.2: Contour plots for $C(\mathbf{h}; u)$ axially symmetric in space ($v_1 = 0.01,\ v_2 = 0$), where $\gamma = 1$, $\nu = d = 2$, $\alpha = 0.02$ and $\beta = 1$. (a) Contour plot of C versus h_1 and h_2 for $u = -10, 0, 10$; (b) contour plot of C versus h_1 and u for all h_2; (c) contour plot of C versus h_2 and u for $h_1 = -200, 0, 200$.

Unlike the covariance function axially symmetric in space, this covariance function moves along a 45 degree line in the spatial domain (Figure 2.3(a)) and along with the axis of u (Figure 2.3(b)). Figure 2.3(b) also says that the ratio of α to β is strongly related to the obliqueness of the shape. The asymmetry vector $\mathbf{v}$ also changes the shape and the centroid (Figure 2.3(c),(d)). Figure 2.4 through 2.6 display the patterns of a covariance function which is asymmetric in space and time. From Figure 2.4, we see that the covariance function does not move along with 45 degree line on spatial domain and the moving speed and the angle of line connecting the centroids are influenced by each element of $\mathbf{v}$ (Figure 2.4(b)-(d)). This figure also shows that the shape changes in comparison to that of a covariance symmetric in time (Figure 2.4(a)). Figure 2.5 and 2.6 illustrate the contour plots of a covariance function asymmetric in space and time versus each spatial lag and u. These figures show that the covariance function moves along with the

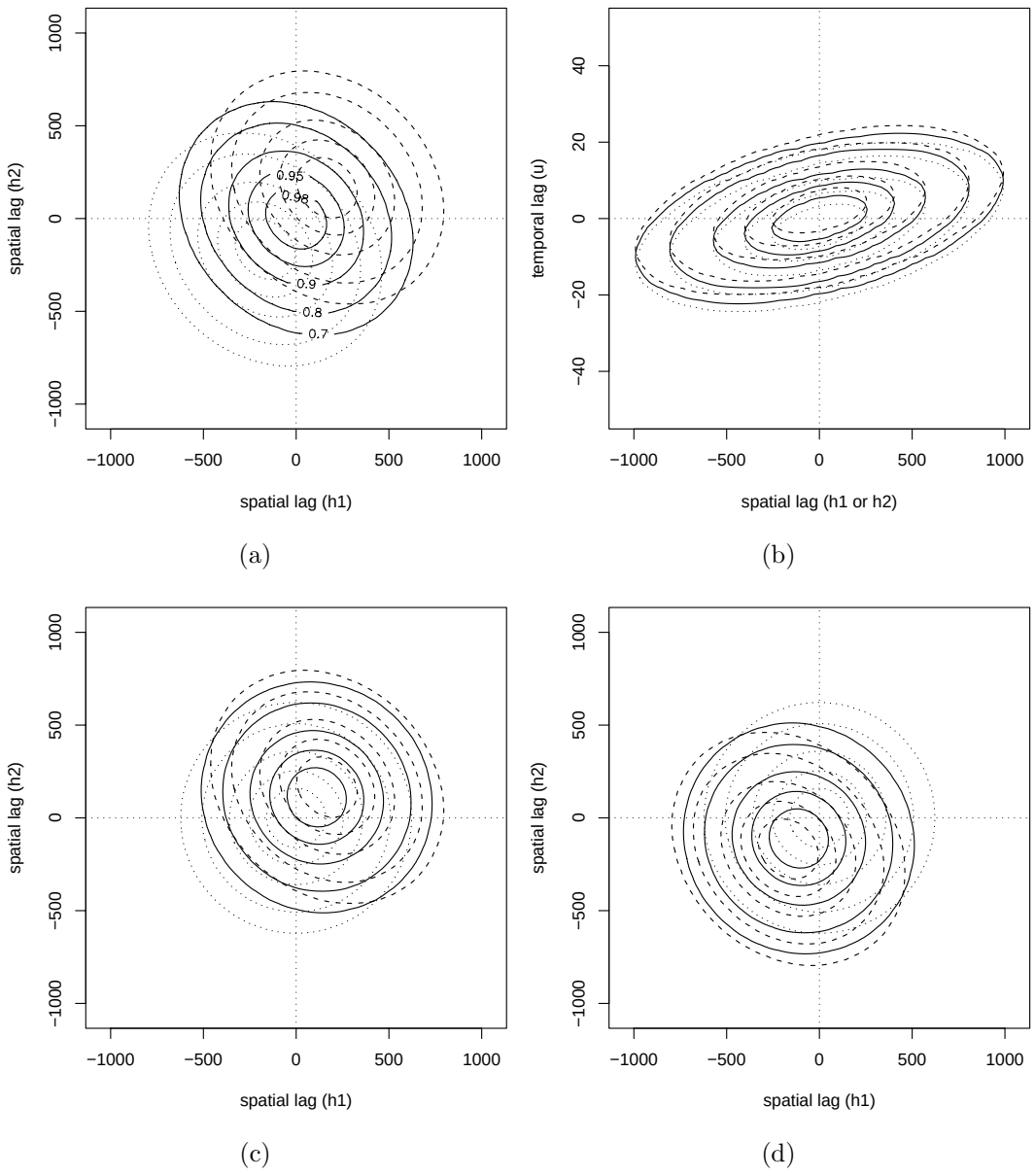

Figure 2.3: Contour plots for $C(\mathbf{h}; u)$ digonally symmetric in space ($v_1 = v_2 = v_0 = 0.01$), where $\gamma = 1$, $\nu = d = 2$, $\alpha = 0.02$ and $\beta = 1$. (a) Contour plot of C versus h_1 and h_2 for $u = -10, 0, 10$; (b) contour plot of C versus h_1 (h_2) and u for h_2 (h_1)$= -200, 0, 200$; (c) contour plot of C versus h_1 and h_2 for $v_0 = 0, 0.005, 0.01$ and $u = 10$; (d) contour plot of C versus h_1 and h_2 for $v_0 = 0, 0.005, 0.01$ and $u = -10$.

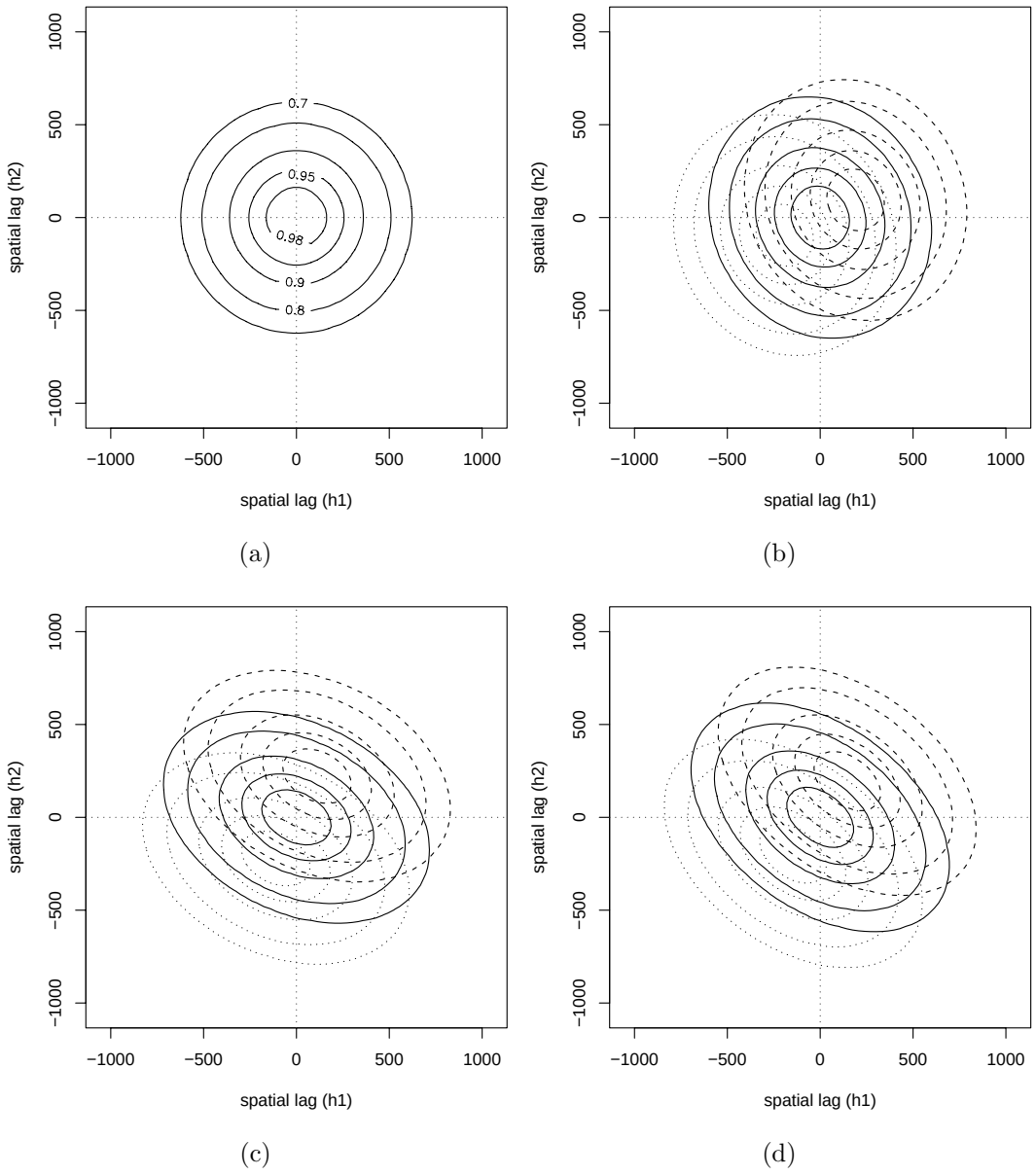

Figure 2.4: Contour plots for $C(\mathbf{h}; u)$ asymmetric in space and time versus h_1 and h_2 for $u = -10, 0, 10$, where $\gamma = 1$, $\nu = d = 2$, $\alpha = 0.02$, and $\beta = 1$. (a) $\mathbf{v} = (0, 0)'$; (b) $\mathbf{v} = (0.01, 0.005)'$; (c) $\mathbf{v} = (0.01, 0.02)'$; (d) $\mathbf{v} = (0.015, 0.02)'$.

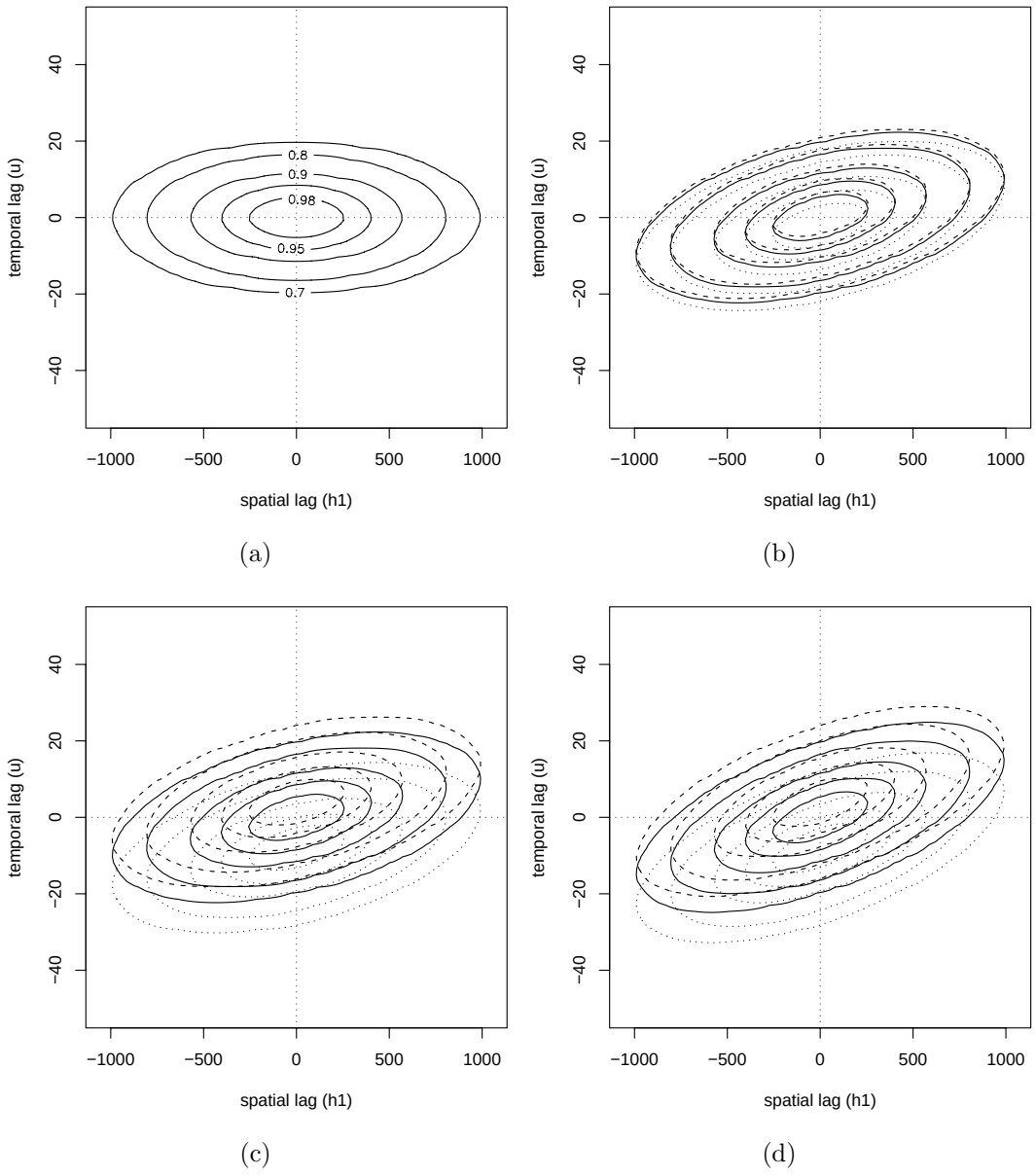

Figure 2.5: Contour plots for $C(\mathbf{h}; u)$ asymmetric in space and time versus h_1 and u for $h_2 = -400, 0, 400$, where $\gamma = 1$, $\nu = d = 2$, $\alpha = 0.02$, and $\beta = 1$. (a) $\mathbf{v} = (0, 0)'$; (b) $\mathbf{v} = (0.01, 0.005)'$; (c) $\mathbf{v} = (0.01, 0.02)'$; (d) $\mathbf{v} = (0.015, 0.02)'$.

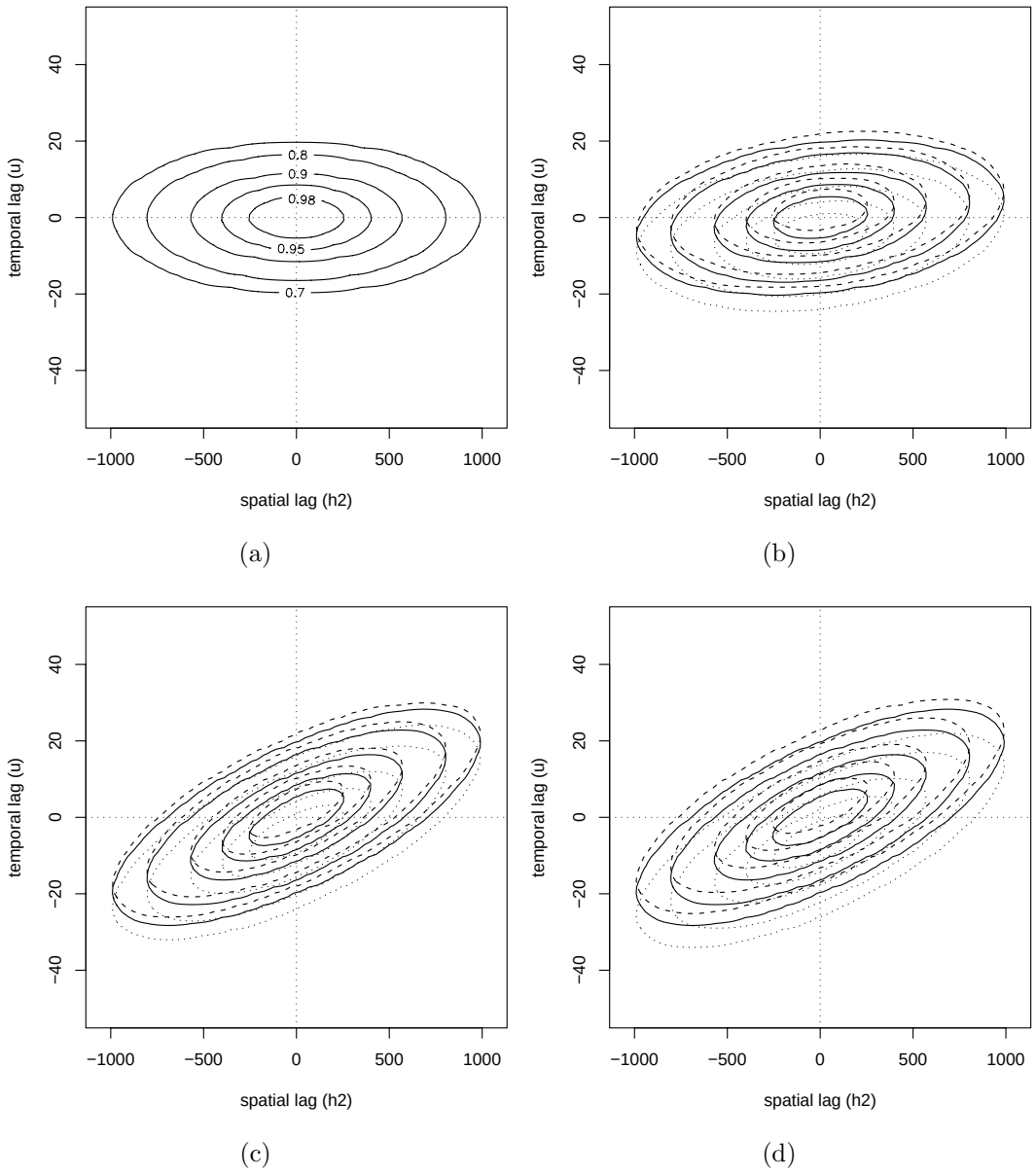

Figure 2.6: Contour plots for $C(\mathbf{h}; u)$ asymmetric in space and time versus h_2 and u for $h_1 = -400, 0, 400$, where $\gamma = 1$, $\nu = d = 2$, $\alpha = 0.02$, and $\beta = 1$. (a) $\mathbf{v} = (0, 0)'$; (b) $\mathbf{v} = (0.01, 0.005)'$; (c) $\mathbf{v} = (0.01, 0.02)'$; (d) $\mathbf{v} = (0.015, 0.02)'$.

axis of u, at different moving speed, which depends on the magnitude of $\mathbf{v}$.

In this section, we have proposed new classes of asymmetric spatial-temporal covariance models by using a valid spectral density function, which guarantees the positive-definiteness of the corresponding covariance function. Symmetry or lack of symmetry are controled by the asymmetry parameter vectors $\mathbf{v}_1$ and $\mathbf{v}_2$ in that magnitude and sign of each element are quitely related to degree and direction of movement in the modeled field. They also play an important role in changing shape of covariance functions. However, the interpretation of asymmetry vectors are different in that the units of $\mathbf{v}_1$ are time divided by distance, that is, the reciprocals of speed, not kinds of velocity whereas the units of $\mathbf{v}_2$ are distance divided by time, which can be called velocities.

2.4 Symmetry and Separability

In this section, we clarify the relationship between symmetry and separability in spatial-temporal processes and, based on a separable spectral density function, extend the models proposed in Section 2.3 to the nonseparable case. Symmetry and separability are the main assumptions that are frequently taken for granted in most applications in the environmental research. The common advantage of symmetry and separability is the simplification attained for modeling purpose. Symmetry and separability in spatial or spatial-temporal processes are highly related to each other.

Taking symmetry and separability into account, we now propose another new class of asymmetric spatial-temporal stationary covariance models, in which separability is a special case. In order to build the covariance functions asymmetric as well as nonseparable, we consider the following spectral density function:

$$\begin{aligned} f_{\mathbf{v}}(\boldsymbol{\omega};\tau) &= \gamma\left(\alpha^2+\|\boldsymbol{\omega}+\tau\mathbf{v}_1\|^2\right)^{-\nu}\left(\beta^2+(\tau+\mathbf{v}_2'\boldsymbol{\omega})^2\right)^{-\nu} \\ &= f_0(\boldsymbol{\omega}+\tau\mathbf{v}_1;\tau+\mathbf{v}_2'\boldsymbol{\omega}), \end{aligned} \tag{2.18}$$

where $f_0(\boldsymbol{\omega};\tau) \equiv \gamma\left(\alpha^2+\|\boldsymbol{\omega}\|^2\right)^{-\nu}\left(\beta^2+\tau^2\right)^{-\nu}$ is the spectral density function transformed from an simple stationary separable covariance function. Based on the setting of (2.18), we can express the corresponding covariance function as

$$\begin{aligned} C_{\mathbf{v}}(\mathbf{h};u) &= \int_{\mathbb{R}^d}\int_{\mathbb{R}} \exp\{i\mathbf{h}'\boldsymbol{\omega}+iu\tau\} f_0(\boldsymbol{\omega}+\tau\mathbf{v}_1;\tau+\mathbf{v}_2'\boldsymbol{\omega})\, d\tau\, d\boldsymbol{\omega} \\ &= \int_{\mathbb{R}^d}\int_{\mathbb{R}} \exp\left\{ i\frac{(\widetilde{\mathbf{h}}-u\mathbf{v}_2)'}{1-\mathbf{v}_1'\mathbf{v}_2}\boldsymbol{\omega} + i\frac{(u-\mathbf{h}'\mathbf{v}_1)}{1-\mathbf{v}_1'\mathbf{v}_2}\tau \right\} \frac{f_0(\boldsymbol{\omega};\tau)}{1-\mathbf{v}_1'\mathbf{v}_2}\, d\tau\, d\boldsymbol{\omega} \\ &= \frac{1}{1-\mathbf{v}_1'\mathbf{v}_2}\, C_{\mathbf{s}}\left(\frac{\widetilde{\mathbf{h}}-u\mathbf{v}_2}{1-\mathbf{v}_1'\mathbf{v}_2}\right) C_T\left(\frac{u-\mathbf{h}'\mathbf{v}_1}{1-\mathbf{v}_1'\mathbf{v}_2}\right), \end{aligned} \tag{2.19}$$

where $C_{\mathbf{s}}$ is two-dimensional spatial covariance function and C_T is one-dimensional temporal covariance function. By direct derivation from (2.19) (see Stein (2005)), we can obtain the closed form of asymmetric nonseparable covariance function given by

$$\begin{aligned} C_{\mathbf{v}}(\mathbf{h};u) =& \frac{1}{1-\mathbf{v}_1'\mathbf{v}_2} \times \frac{\gamma\pi^{(d+1)/2}\alpha^{-2\nu+d}\beta^{-2\nu+1}}{2^{\nu-(d+1)/2-2}\Gamma^2(\nu)} \\ & \times \mathcal{M}_{\nu-d/2}\left(\alpha\left\|\frac{\widetilde{\mathbf{h}}-u\mathbf{v}_2}{1-\mathbf{v}_1'\mathbf{v}_2}\right\|\right)\mathcal{M}_{\nu-1/2}\left(\beta\left|\frac{u-\mathbf{h}'\mathbf{v}_1}{1-\mathbf{v}_1'\mathbf{v}_2}\right|\right). \end{aligned} \tag{2.20}$$

From (2.20), we can see that the asymmetry vectors $\mathbf{v}_1$ and $\mathbf{v}_2$ control separability as well as symmetry. Under the setting of (2.19), the following types of symmetry are defined:

T.1* axial symmetry in time and separable if $\mathbf{v}_1 = \mathbf{v}_2 = \mathbf{0}$

T.2* axial symmetry in space but nonseparable if $v_{11} \neq 0$ or $v_{21} \neq 0$ and $v_{12} = v_{22} = 0$

T.3* diagonal symmetry in space but nonseparable if $v_{11} = v_{12} \neq 0$ and $v_{21} = v_{22} \neq 0$

T.4* asymmetry in space and time, and nonseparable otherwise.

As forementioned, the main difference between the two asymmetric covariance models, (2.12) in Section 2.3 and (2.19) is whether separability can be a special case or not. (2.12) is always nonseparable for all posssible $\mathbf{v} \in \mathbb{R}^d$ whereas (2.19) can be separable (see **T.1***). By the similar way that we applied in the previ-

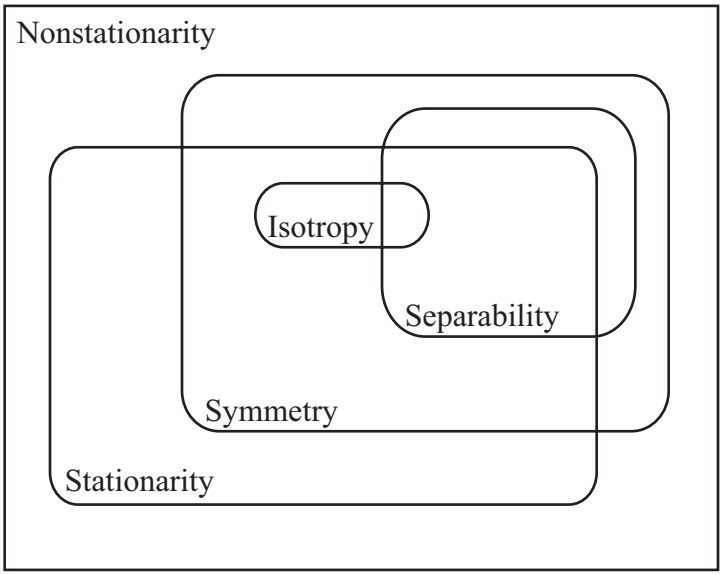

Figure 2.7: Relationship between symmetry and separability

ous class denoted in (2.12), we can also consider the following two asymmetric

nonseparable spatial-temporal covariance models:

$$C_{\mathbf{v}_1}(\mathbf{h};u) = \frac{\gamma\pi^{(d+1)/2}\alpha^{-2\nu+d}\beta^{-2\nu+1}}{2^{\nu-(d+1)/2-2}\Gamma^2(\nu)}\mathcal{M}_{\nu-d/2}\left(\alpha\|\mathbf{h}\|\right)\mathcal{M}_{\nu-1/2}\left(\beta|u-\mathbf{h}'\mathbf{v}_1|\right), \quad (2.21)$$

and

$$C_{\mathbf{v}_2}(\mathbf{h};u) = \frac{\gamma\pi^{(d+1)/2}\alpha^{-2\nu+d}\beta^{-2\nu+1}}{2^{\nu-(d+1)/2-2}\Gamma^2(\nu)}\mathcal{M}_{\nu-d/2}\left(\alpha\|\mathbf{h}-u\mathbf{v}_2\|\right)\mathcal{M}_{\nu-1/2}\left(\beta|u|\right). \quad (2.22)$$

The corresponding spectral density functions are, respectively, given by

$$\begin{aligned} f_{\mathbf{v}_1}(\boldsymbol{\omega};\tau) &= \gamma\left(\alpha^2+\|\boldsymbol{\omega}+\tau\mathbf{v}_1\|^2\right)^{-\nu}\left(\beta^2+\tau^2\right)^{-\nu} \\ &= f_0(\boldsymbol{\omega}+\tau\mathbf{v}_1;\tau), \end{aligned} \quad (2.23)$$

and

$$\begin{aligned} f_{\mathbf{v}_2}(\boldsymbol{\omega};\tau) &= \gamma\left(\alpha^2+\|\boldsymbol{\omega}\|^2\right)^{-\nu}\left(\beta^2+(\tau+\mathbf{v}_2'\boldsymbol{\omega})^2\right)^{-\nu} \\ &= f_0(\boldsymbol{\omega};\tau+\mathbf{v}_2'\boldsymbol{\omega}). \end{aligned} \quad (2.24)$$

Now we visualize the relationship among separability, symmetry, stationarity in the spatial-temporal setting. Figure 2.7 displays the Venn diagram describing how these fundamental characteristics are mutually related to one another. As one can see, symmetry and separability are mostly overlapped with stationarity although separable covariance models (Fuentes *et al.* 2005) and symmetric ones can be extended to nonstationary case. What is interesting here is that separability can possibly be a subset of symmetry, especially in terms of the covariance function presented in (2.19). posssible expressions of a spectral density function yielding a nonstationary symmetric covariance function are as follow:

$$f_{\mathbf{s}_j}(\boldsymbol{\omega};\tau) = \gamma_j\left(\alpha_j^2\beta_j^2+\beta_j^2\|\boldsymbol{\omega}+\tau\mathbf{v}_1\|^2+\alpha_j^2(\tau+\mathbf{v}_2'\boldsymbol{\omega})^2\right)^{-\nu_j},$$

or

$$f_{\mathbf{s}_j}(\boldsymbol{\omega};\tau) = \gamma_j \left(\alpha_j^2 + \|\boldsymbol{\omega} + \tau \mathbf{v}_1\|^2\right)^{-\nu_j} \left(\beta_j^2 + (\tau + \mathbf{v}_2'\boldsymbol{\omega})^2\right)^{-\nu_j},$$

where $j = 1, \cdots, k$ is the index of subregion satisfying stationarity, and $\mathbf{s}_j$ is the center of the j-th subregion.

2.5 Real Application

In this section, we apply the class of asymmetric stationary spatial-temporal covariance models to an air-pollution dataset, which is $PM_{2.5}$ daily concentration aquired by the U.S. Environmental Protection Agency (EPA)'s Federal Reference Method (FRM) monitoring stations. The main reason why we are interested in $PM_{2.5}$ concentrations is that this air-pollutant is one of the important factors in the public health problem and, according to many environmenal studies, has complex spatial or spatial-temporal dependency structure (Zidek (1997) and Golam Kibria *et al.* (2002)). The spatial domain for this dataset is the northeastern U.S (Figure 2.8), which is almost the same region as the northeastern census division. The measurements were obtained from August 1st to August 31st, 2003. First we remove spatial trend by considering the second order polynomial function with geodesic distances transformed from the orginal longitudes and latitudes in order to take the earth's curvature into account.

Now we briefly introduce the weighted least squares (WLS) estimation method which can be applied to asymmetric spatial-temporal covariance models. Let

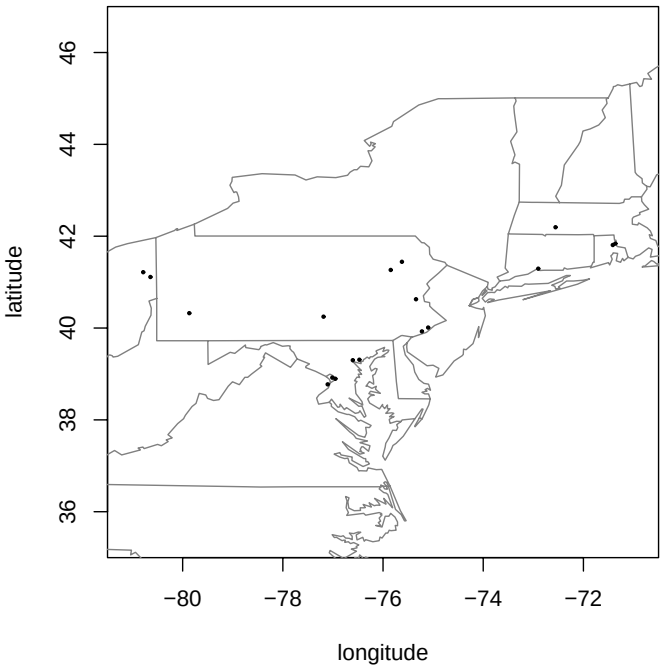

Figure 2.8: The map of the 18 monitoring stations in the northeastern U.S.

$Z(\mathbf{s}_i, t)$ be the observed $PM_{2.5}$ concentration for time t at site i; $t = 1, \cdots, 31$, $i = 1, \cdots, 18$, and $X(\mathbf{s})$ and $Y(\mathbf{s})$ be the geodesic distances with unit of kilometers. Then we consider the spatial-temporal structure as follows:

$$Z(\mathbf{s}_i, t) = g(X(\mathbf{s}_i), Y(\mathbf{s}_i)|\boldsymbol{\delta}) + \epsilon(\mathbf{s}_i, t),$$

where g is the second-order polynomial function with coefficient parameters $\boldsymbol{\delta}$, $\boldsymbol{\epsilon} \sim MN(\mathbf{0}, \sigma\mathbf{I} + \boldsymbol{\Sigma}(\boldsymbol{\theta}))$, σ is the nugget effect, and $\boldsymbol{\theta} = (\phi, \alpha, \beta, \mathbf{v}_1', \mathbf{v}_2')'$, where ϕ is a partial sill. The variance-covariance matrix $\boldsymbol{\Sigma}(\boldsymbol{\theta})$ is based on the following Gaussian covariance functions:

M.1 $C_0(\mathbf{h}; u) = \phi \exp\left\{\alpha^2 \|\mathbf{h}\|^2 + \beta^2 u^2\right\}$

M.2 $C_{\mathbf{v}_1}(\mathbf{h}; u) = \phi \exp\left\{\alpha^2 \|\mathbf{h}\|^2 + \beta^2 (u - \mathbf{v}_1'\mathbf{h})^2\right\}$

M.3 $C_{\mathbf{v}_2}(\mathbf{h};u) = \phi \exp\left\{\alpha^2\|\mathbf{h} - u\mathbf{v}_2\|^2 + \beta^2 u^2\right\}$

M.4 $C_{\mathbf{v}}(\mathbf{h};u) = \dfrac{\phi}{1-\mathbf{v}_1'\mathbf{v}_2} \exp\left\{(1-\mathbf{v}_1'\mathbf{v}_2)^{-2}\left(\alpha^2\|\widetilde{\mathbf{h}} - u\mathbf{v}_2\|^2 + \beta^2(u-\mathbf{v}_1'\mathbf{h})^2\right)\right\}$.

In order to estimate the covariance parameters, $\boldsymbol{\Theta} = (\sigma, \boldsymbol{\theta}')'$, we propose the empirical spatial-temporal semivariogram, $\widehat{\gamma}(\mathbf{h}(p,q);u)$ given by

$$\widehat{\gamma}(\mathbf{h}(p,q);u) \equiv \frac{1}{N(\mathbf{h}(p,q);u)} \sum_{(i,j,t,t^*)\in N(\mathbf{h}(p,q);u)} \left(\widetilde{Z}(\mathbf{s}_i,t) - \widetilde{Z}(\mathbf{s}_j,t^*)\right)^2, \qquad (2.25)$$

where

$$N(\mathbf{h}(p,q);u) \equiv \{(i,j,t,t^*) : \mathbf{s}_i - \mathbf{s}_j \in \mathcal{T}(\mathbf{h}(p,q)); |t-t^*| = u\},$$

$$\{\mathbf{h}(p,q)\} = \{-h_1(P), \cdots, -h_1(1), 0, \cdots, h_1(P)\}$$
$$\times \{-h_2(Q), \cdots, -h_2(1), 0, \cdots, h_2(Q)\},$$

and $\widetilde{Z}(\mathbf{s},t) = Z(\mathbf{s},t) - g\left(X(\mathbf{s}), Y(\mathbf{s})|\widehat{\boldsymbol{\delta}}\right)$ and $\widehat{\boldsymbol{\delta}}$ is the oridinary least squares (OLS) estimator. Here $\mathcal{T}(\mathbf{h}(p,q))$ is prespecified tolerance region with centroid of $\mathbf{h}(p,q)$. Then the weighted-least squares (WLS) method (see Cressie (1993), pp.96) based on the empirical semivariogram in (2.25) is employed to obtain the estimates of the covariance parameters, $\boldsymbol{\Theta}$, which minimize the weighted sum of squares error (WSSE), which is defined as

$$W(\boldsymbol{\Theta}) \equiv \sum_{p=-P}^{P}\sum_{q=-Q}^{Q}\sum_{u=0}^{U} |N(\mathbf{h}(p,q);u)| \left\{\frac{\widehat{\gamma}(\mathbf{h}(p,q);u)}{\gamma(\mathbf{h}(p,q);u|\boldsymbol{\Theta})} - 1\right\}^2, \qquad (2.26)$$

where $\gamma(\mathbf{h}(p,q);u|\boldsymbol{\Theta})$ is the theoretical spatial-temporal semivariogram with parameters $\boldsymbol{\Theta}$. Here $h_j(p) \equiv \{2I_{(p>0)} - 1\} \times h_j(|p|)$ for $j = 1, 2$ where $I_{(\cdot)}$ is an

indicator function. We also consider the maximum likelihood (ML) estimation method for obtaining the covariance parameter estimates.

Now we explain the result from the analysis of $PM_{2.5}$ daily concentration dataset. The parameter estimation methods are performed with the spatially detrended $PM_{2.5}$ concentrations, $\{\widetilde{Z}(\mathbf{s}, t)\}$. In order to gain some computational benefit, we employ the estimates from the WLS method as initial values for obtaining the estimates from the ML method. The WSSE in (2.26) and the negative log-likelihood are minimized using the routine optim in R. The Table 2.2 shows the estimates of $\boldsymbol{\Theta}$ from the WLS and the ML methods for each model (see **M.1** through **M.4**). As one can see, there does not exist any big difference of parameter estimates between the estimation methods for all the models. The estimates for the components of $\mathbf{v}_1$ in **M.2** have the same signs as those of $\mathbf{v}_2$ in **M.3** regardless of the estimation methods. What is interesting here is that the signs of the estimates for the last two components, v_{21} and v_{22} in **M**.**4** are opposite to the ones in **M**.**3**. One possible reason is that, as we mentioned before, the parameter vectors $\mathbf{v}_1$, $\mathbf{v}_2$ and $\mathbf{v}$ control the shape of a spatial-temporal covariance function as well as symmetry or lack of symmetry inherent in spatial-temporal processes. So, the shape of the asymmetric covariance function employed in **M**.**4** is determined by adjustments from v_{11} and v_{21}, and from v_{12} and v_{22}. From the WSSE and the negative log-likelihoods based on the estimates from the corresponding methods, we can know that, as the number of parameters increases, the given dataset gets explained well though the simple model **M**.**1** is not always bad from point of view

of information citerion.

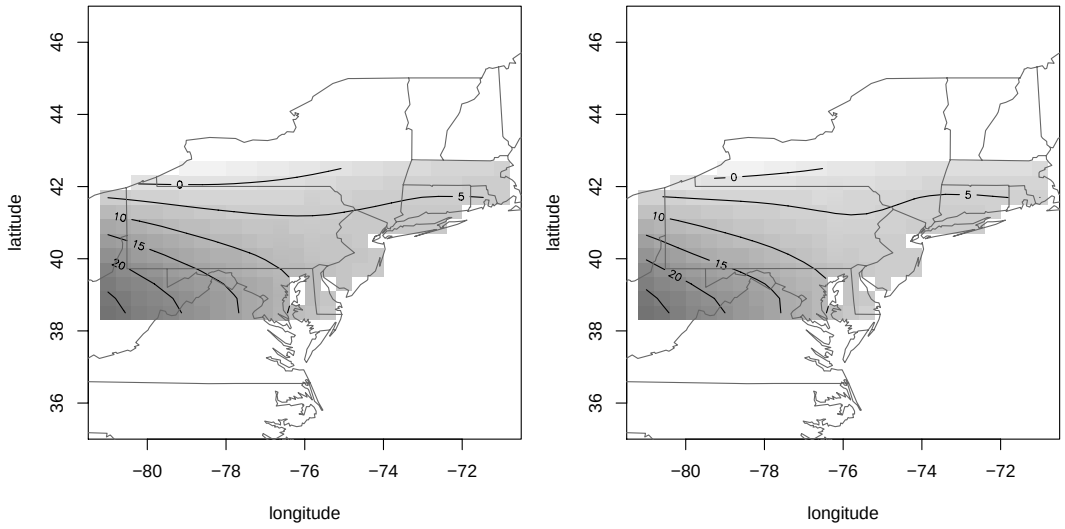

(a) **M.1** (b) **M.2**

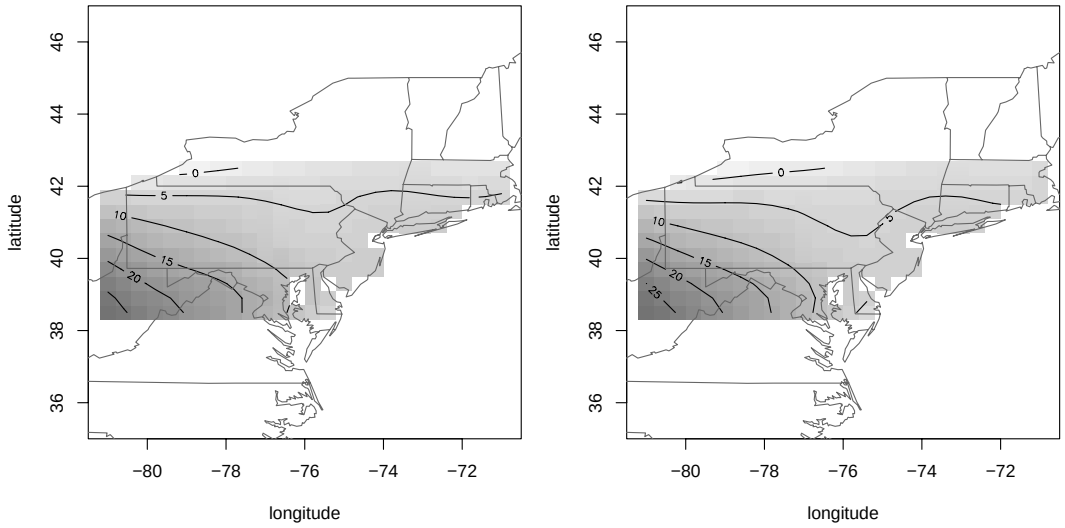

(c) **M.3** (d) **M.4**

Figure 2.9: Kriging maps based on the ML estimates in Table 2.2 for each model. Note that the interpolation is performed at the regular grids on August 31, 2003.

Based on the ML estimates for each model, we predict the $PM_{2.5}$ concentrations at the preassigned grids on August 31, 2003. As you can see from Figure 2.9,

Table 2.1: Square-root of mean squared prediction errors based on the WLS and the ML estimation methods at the two reserved stations.

Station	**M.1**		**M.2**		**M.3**		**M.4**	
	WLS	ML	WLS	ML	WLS	ML	WLS	ML
#1.	1.984	1.995	2.002	2.025	1.975	2.043	1.984	2.002
#2.	3.452	3.370	3.480	3.235	3.473	3.143	3.489	3.270

the prediction patterns are quite similar except portion of the region having the negative predicted values. That is, **M.2** through **M.4** can be preferred to **M.1** in that only nonnegative $PM_{2.5}$ concentrations are measured in pratice.

Now we evaluate the performances of the asymmetric spatial-temporal covariance models, **M.1** through **M.4** by means of the classical cross-validation technique. We first remove two stations from the spatial domain of our interest, analyze the data from the remaining stations, and compare the observed values at the reserved stations with the predicted ones based on the estimation. Table 2.1 shows the square-root of mean squared prediction errors (RMSPE) at each reserved station for every estimation method. In terms of the RMSPE, **M.3** is slightly better than the other asymmetric covariance models (**M.2** and **M.4**) except the case of the ML estimation for the first reserved station although there is no clear evidence that the general asymmetric covariance models (**M.2**-**M.4**)yield more reliable predictions than the symmetric model (**M.1**), that is, the model with $\mathbf{v}_1 = \mathbf{v}_2 = \mathbf{0}$. Based on the predictions from the classical cross-validation technique, Figure 2.10 and Figure 2.11 display the scatterplots of the observed

values and the corresponding predicted values based on the ML estimates for each reserved station. As one can see from these two figures, there is not any big difference of the relationship between the observations and the corresponding predictions among the covariance models and the prediction at the first reserved station is done much better than the prediction at the second reserved station, where every model produces slightly overestimated predicted values in comparison to the observations.

In this section, we have applied a new class of asymmtric spatial-temporal covariance models to the $PM_{2.5}$ daily concentrations at the FRM monitoring stations in the northeastern U.S. From the data analysis, we can know that the spatial-temporal processes based on asymmetric covariance functions explain the given dataset better than the process based on simple covariance function in terms of the WSSE and the likelihood whereas, for the performance of prediction matter, the number of stations is not enough for an asymmetric covariance function to capture the spatial-temporal dependency structures.

2.6 Discussion

In this chapter, we introduced new concepts of symmetry in spatial-temporal processes and proposed classes of asymmetric stationary spatial-temporal covariance models. Since these covariances are just Fourier transformations of the corresponding valid spectral density functions, they can easily be shown to be positive

definite. Unlike a process with separable, even nonseparable covariance, an asymmetric spatial-temporal proecess is influenced by spatial-temporal dependencies, which are mainly controled by asymmetry parameters. This characteristic is very helpful to analyze the air-pollution data affected by some external metheological conditions, for instance, wind speed, wind direction, air pressure and so on.

The asymmetric covariance models can be extended to the spatial domain with $d > 2$ although our results presented in this study are based on the two dimensional spatial domain. For example, in case of spatial domain with longitude, latitude and altitude, the asymmetric covariance models are constructed in $\mathbb{R}^3 \times \mathbb{R}$. As part of our further research, we are estimating the parameters by means of Bayesian approach taking into account uncertainties in the covariance models.

Table 2.2: Parameter Estimates based on Gaussian Asymmetric Spatial-Temporal Covariance from WLS and ML methods. Note that $(-4) \equiv 10^{-4}$.

$\boldsymbol{\Theta}$	**M.1**		**M.2**		**M.3**		**M.4**	
	WLS	ML	WLS	ML	WLS	ML	WLS	ML
σ	5.920	5.935	6.046	5.748	5.637	5.111	5.517	4.259
ϕ	105.7	105.3	106.5	105.3	105.5	105.5	103.2	109.2
α	0.003	0.003	0.003	0.004	0.003	0.004	0.003	0.005
β	0.838	0.888	0.842	0.847	0.826	0.800	0.821	0.978
v_{11}			6.(-4)	1.(-4)			1.(-3)	2.(-3)
v_{12}			-6.(-4)	-3.(-4)			-1.(-3)	1.(-3)
v_{21}					20.07	20.07	-59.84	-59.82
v_{22}					-45.10	-45.10	-59.98	-59.81
WSSE	686.1		641.1		678.8		580.4	
$-\log(L)$		1617		1613		1613		1608

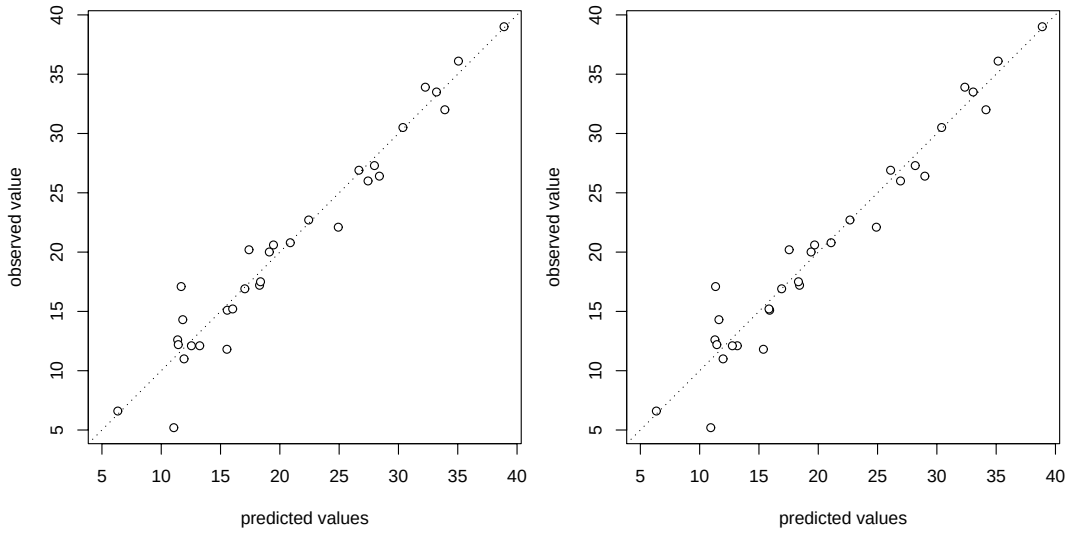

(a) **M.1** (b) **M.2**

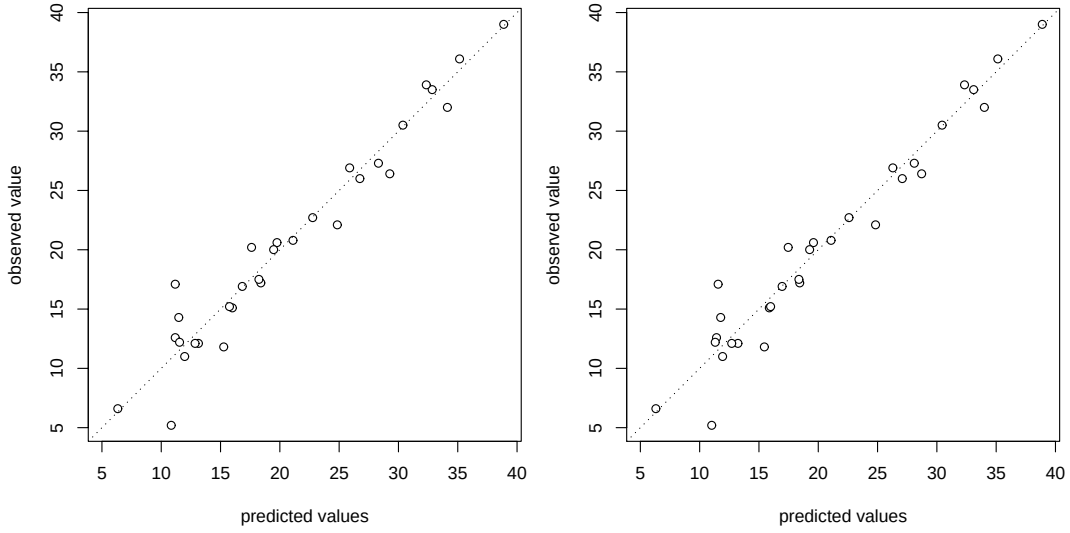

(c) **M.3** (d) **M.4**

Figure 2.10: Scatter plots of the observed values at the first reserved station and the ML predicted values obtained from each covariance model. Note that the dashed line stands for the perfect relationship.

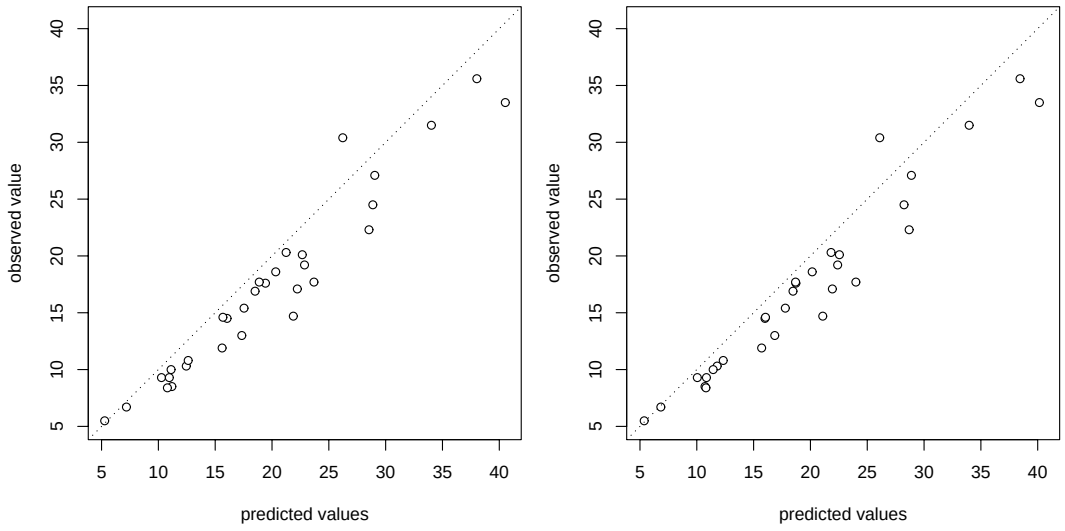

(a) **M.1** (b) **M.2**

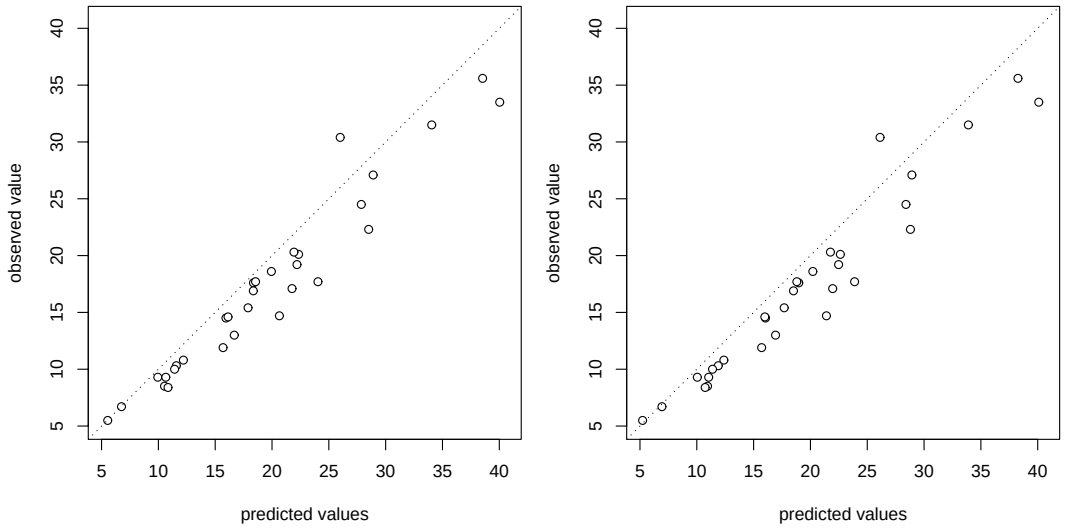

(c) **M.3** (d) **M.4**

Figure 2.11: Scatter plots of the observed values at the second reserved station and the ML predicted values obtained from each covariance model. Note that the dashed line stands for the perfect relationship.

Chapter 3

Testing Lack of Symmetry in Spatial-Temporal Processes

3.1 Introduction

Symmetry and separability are the main assumptions used in spatial statistics about a covariance function. Symmetry and separability in spatial or spatial-temporal processes are highly related to each other. Separability provides many advantages, such as the simplified representation of the covariance matrix and, consequently, important computational benefits. Symmetry is related to the spatial or spatial-temporal dependencies. This characteristic has been assumed because of mathematical convenience, modeling parsimony or calculational efficiency. The common advantage of symmetry and separability is the simplification attained for modeling purpose. However, many studies in environmental sciences show that real data have such complex spatial-temporal dependency structures that are diffi-

cult to model and estimate by using just separability, symmetry or other standard assumptions of the covariance function.

Lots of research about separability has been done so far while symmetry has not been in the spotlight yet. Modeling nonseparable covariance functions is one of the keys for the more reliable prediction in the environmental research fields. Cressie and Huang (1999) introduce a new class of nonseparable, spatial-temporal stationary covariance functions with space-time interaction, which have the separable covariance function as a special case. Gneiting (2002) also proposes general classes of nonseparable, stationary spatial-temporal covariance functions which are directly constructed in the space-time domain and are based on Fourier-free implementation. Fuentes *at al.* (2005) propose a new class of nonseparable and nonstationary spatial-temporal covariance models, which have a unique parameter indicating spatial-temporal dependency. In addition to the modeling issue, many studys about testing lack of separability have been accomplished. Shitan and Brockwell (1995) use an asymptotic χ^2 test for stationary spatial autoregressive processes. Guo and Billard (1998) propose the Wald test for testing lack of a doubly-geometric process under the temporal setting. A likelihood ratio test for lack of separability for $i.i.d$ multivariate processes is proposed by Mitchell (2002), and Mitchell *et al.* (2002). Fuentes (2006) developes a formal test for lack of separability and lack of stationarity of spatial-temporal covariance functions by applying a two-factor analysis of variance (ANOVA) procedure, which is applicable to more general spatial-temporal covariance models.

The most relevant works about symmetry have been done by Scaccia and Martin (2005), and Lu and Zimmerman (2005). For a spatial process, $\{Z(\mathbf{s}) : \mathbf{s} = (s_1, s_2)' \in \mathbb{D} \subset \mathbb{R}^2\}$, especially for two-dimensional rectangular lattice data Scaccia and Martin (2005) developed new tests of axial symmetry and separability which are, respectively, defined by

$$C(h_1, h_2) = C(-h_1, h_2), \quad \forall h_1, h_2,$$

and

$$C(h_1, h_2) = C(h_1) \cdot C(h_2), \quad \forall h_1, h_2,$$

where $C(h_1, h_2) \equiv \mathrm{Cov}\left(Z(s_1 + h_1, s_2 + h_2), Z(s_1, s_2)\right)$, h_1 and h_2 are the first and the second spatial lags. Their tests are performed in two stages: testing axial symmetry first and then, if the hypothesis of axial symmetry is not rejected, testing separability. Under an $n_1 \times n_2$ rectangular lattice data, their tests are based on the periodogram denoted by

$$I(\omega_1, \omega_2) = \frac{1}{(2\pi)^2} \sum_{h_1=-n_1+1}^{n_1-1} \sum_{h_2=-n_2+1}^{n_2-1} C(h_1, h_2) \cos(h_1\omega_1 + h_2\omega_2).$$

One of the tests concerned in this paper is as following:

$$D = -2 \sum_{\omega_1, \omega_2} \left[\log \frac{I(\omega_1, \omega_2)}{\bar{I}(\omega_1, \omega_2)} + \log \frac{I(\omega_1, -\omega_2)}{\bar{I}(\omega_1, \omega_2)} \right],$$

where $\bar{I}(\omega_1, \omega_2) = [I(\omega_1, \omega_2) + I(\omega_1, -\omega_2)]/2$. Lu and Zimmerman (2005) also proposed diagnostic tests of axial symmetry and complete symmetry which is defined by

$$C(h_1, h_2) = C(-h_1, h_2) = C(-h_2, h_1) = C(h_2, h_1), \quad \forall h_1, h_2.$$

Their tests of symmetries are also based on certain ratios of spatial periodograms. These noteworthy studies, however, are only applicable for spatial processes, not spatial-temporal ones. The extension of symmetry to spatial-temporal processes has been tried by Stein (2005), who proposes spatial-temporal covariance models with lack of full symmetry (see Gneiting (2002)). His approach is based on generating asymmetric models from symmetric ones by taking derivatives. No formal tests for lack of symmetry in spatial-temporal processes have been developed yet. In this study we propose new formal tests by using spectral representations of the covariance function. The advantage of the tests is that simple analysis of variance (ANOVA) approaches are employed for detecting lack of symmetry inherent in spatial-temporal processes (see Fuentes (2006)).

This chapter is organized as follows. In Section 3.2, we introduce the spectral representation under the spatial-temporal setting. Based on the spectral representation, we propose new tests for lack of symmetry in spatial-temporal processes in Section 3.3. In Section 3.4 and Section 3.5, the performances of the tests are evaluated by simulation study and by the analysis of air pollution data. Finally we briefly discuss our approach in Section 3.6.

3.2 Spectral Representation of Stationary Spatial-Temporal Processes

In this section, we talk about the spectral representation of stationary spatial-temporal processes, which is a major key for building new tests for lack of symmetry. A stationary spatial-temporal process $\{Z(\mathbf{s};t) : \mathbf{s} \in \mathbb{D} \subset \mathbb{R}^d; t \in \mathbb{T} \subset \mathbb{R}\}$ can be expressed in the spectral domain by sinusoidal forms with different frequencies $(\boldsymbol{\omega}, \tau)$, where $\boldsymbol{\omega}$ is d-dimensional spatial frequency, and τ is temporal frequency. If $Z(\mathbf{s},t)$ is a stationary spatial-temporal process with the corresponding covariance $C(\mathbf{h};u)$, then we can rewrite the process in the following Fourier-Stieltjes integral (Yaglom (1987)):

$$Z(\mathbf{s},t) = \int_{\mathbb{R}^d}\int_{\mathbb{R}} \exp(i\mathbf{s}'\boldsymbol{\omega} + i\tau t)\, dY(\boldsymbol{\omega},\tau),$$

where Y is a random process with complex symmetry except for the constraint, $dY(\boldsymbol{\omega},\tau) = dY^c(-\boldsymbol{\omega},-\tau)$, which ensures that $Z(\mathbf{s};t)$ is real-valued. Using the spectral representation of Z, the covariance function $C(\mathbf{h};u)$ can be represented as

$$C(\mathbf{h};u) = \int_{\mathbb{R}^d}\int_{\mathbb{R}} \exp(i\mathbf{h}'\boldsymbol{\omega} + i\tau u)\, G(d\boldsymbol{\omega};d\tau), \tag{3.1}$$

where $(\mathbf{h};u) = (\mathbf{s}_i - \mathbf{s}_j; t_k - t_l)$ for $\{\mathbf{s}_i,\mathbf{s}_j\} \subset \mathbb{D}$ and $\{t_k,t_l\} \subset \mathbb{T}$, and the function G is a positive finite measure called the spectral measure or spectral distribution function for Z. The spectral measure G is the expected squared modulus of the process Y denoted by

$$E\{|Y(\boldsymbol{\omega},\tau)|^2\} = G(\boldsymbol{\omega};\tau).$$

We can easily see that $C(\mathbf{h}; u)$ in (3.1) is always positive definite for any finite positive measure G. If G has a density with respect to Lebesgue measure, the spectral density g is the Fourier transform of the spatial-temporal covariance function:

$$g(\boldsymbol{\omega}; \tau) = \frac{1}{(2\pi)^{d+1}} \int_{\mathbb{R}} \int_{\mathbb{R}^d} \exp(-i\mathbf{h}'\boldsymbol{\omega} - i\tau u) C(\mathbf{h}; u)\, d\mathbf{h}\, du, \tag{3.2}$$

and the corresponding covariance function is given by

$$C(\mathbf{h}; u) = \int_{\mathbb{R}^d} \int_{\mathbb{R}} \exp(i\mathbf{h}'\boldsymbol{\omega} + i\tau u)\, g(\boldsymbol{\omega}; \tau)\, d\boldsymbol{\omega}\, d\tau. \tag{3.3}$$

3.3 Tests for Lack of Symmetry In Spatial-Temporal Processes

In Section 3.2, we summarized the spectral representation of a stationary spatial-temporal processes. Now we talk about new tests for lack of symmetry in spatial-temporal processes based on the spectral representation. Before going further, we define three types of symmetry under the spatial-temporal setting. For a stationary spatial-temporal process, $\{Z(\mathbf{s}, t) : \mathbf{s} \in \mathbb{D} \subset \mathbb{R}^d; t \in [0, \infty)\}$, we can define the covariance as follows:

$$\mathrm{Cov}\{Z(\mathbf{s}_i, t_k), Z(\mathbf{s}_j, t_l)\} = C(\mathbf{s}_i - \mathbf{s}_j; t_k - t_l) \equiv C(\mathbf{h}; u), \tag{3.4}$$

where $\mathbf{h} = (h_1, h_2, \cdots, h_d)'$ and u are called spatial lags and time lag, respectively. Based on (3.4), we can define the types of symmetry.

Definition 3.3.1 *A process is called axially symmetric in time if for any temporal*

lag $u \neq 0$*,*

$$C(\mathbf{s}_i - \mathbf{s}_j; u) = C(\mathbf{s}_{i^*} - \mathbf{s}_{j^*}; -u), \tag{3.5}$$

for arbitrary four locations (i, j, i^*, j^*) *satisfying* $\mathbf{s}_i - \mathbf{s}_j = \mathbf{s}_{i^*} - \mathbf{s}_{j^*}$*.*

Under stationarity in space, (3.5) is reduced to

$$C(\mathbf{h}; u) = C(\mathbf{h}; -u), \tag{3.6}$$

where $\mathbf{s}_i = \mathbf{s}_j + \mathbf{h}$ and $\mathbf{s}_{i^*} = \mathbf{s}_{j^*} + \mathbf{h}$. What is important in (3.5) and (3.6) is that the directions and the distances on spatial domain are the same, and the time lags have the same magnitudes but different signs. The second type of symmetry is axial symmetry in space.

Definition 3.3.2 *A process is called (k) axially symmetric in space if*

$$C(\mathbf{h}; u) = C(\mathring{\mathbf{h}}; u), \tag{3.7}$$

where $\mathring{\mathbf{h}} = (h_1, \cdots, h_{k-1}, -h_k, h_{k+1}, \cdots, h_d)'$ *for* k *fixed.*

As can be seen in (3.7), for temporal lag u fixed, all the spatial lags are the same except one spatial lag, which has a different sign. For example, $\mathring{\mathbf{h}} = (-h_1, h_2)'$ is one possible case in case of $d = 2$. The last one is diagonal symmetry in space.

Definition 3.3.3 *A process is called (k-l) diagonally symmetric in space if*

$$C(\mathbf{h}; u) = C(\ddot{\mathbf{h}}; u), \tag{3.8}$$

where $\ddot{\mathbf{h}} = (h_1, \cdots, h_{k-1}, h_l, h_{k+1}, \cdots, h_{l-1}, h_k, h_{l+1}, \cdots, h_d)'$ *for* $k \neq l$*.*

From (3.8) we can see that only two spatial lags, h_k and h_l, are switched with each other. Provided that $d = 2$, $\ddot{\mathbf{h}} = (h_2, h_1)'$.

3.3.1 Test for Lack of Axial Symmetry in Time

Now we explain the analytical aspect of axial symmetry in time (Definition 3.3.1) in spatial-temporal process. By Bochner's theorem, we can always write the positive-definite spatial-temporal covariance in (3.3) in terms of the corresponding valid spectral density function, g in (3.2):

$$C(\mathbf{h};u) = \int_{\mathbb{R}} \int_{\mathbb{R}^d} \exp\{i\mathbf{h}'\boldsymbol{\omega} + iu\tau\} g(\boldsymbol{\omega};\tau)\, d\boldsymbol{\omega}\, d\tau.$$

If C is integrable, then (3.2) can be expressed as

$$\begin{aligned} g(\boldsymbol{\omega};\tau) &= (2\pi)^{-(d+1)} \int_{\mathbb{R}} \int_{\mathbb{R}^d} \exp\{-i\mathbf{h}'\boldsymbol{\omega} - iu\tau\} C(\mathbf{h};u)\, d\mathbf{h}\, d\tau \\ &= (2\pi)^{-d} \int_{\mathbb{R}^d} \exp\{-i\mathbf{h}'\boldsymbol{\omega}\} f(\mathbf{h};\tau)\, d\mathbf{h}, \end{aligned}$$

where for $\mathbf{h}$ fixed and $\tau \in [0,\infty)$, $f(\mathbf{h};\tau)$ is called the cross-spectral density function of $Z(\mathbf{a},t)$, and $Z(\mathbf{a}+\mathbf{h},t)$ and is defined as follows:

$$f(\mathbf{h};\tau) = (2\pi)^{-1} \int_{\mathbb{R}} \exp\{-iu\tau\} C(\mathbf{h};u)\, du = f^c(-\mathbf{h};\tau), \tag{3.9}$$

where the complex conjugate of $f(\mathbf{h};\tau)$, $f(-\mathbf{h};\tau)$ is represented as

$$\begin{aligned} f(-\mathbf{h};\tau) &= (2\pi)^{-1} \int_{\mathbb{R}} \exp\{-iu\tau\} C(-\mathbf{h};u)\, du = (2\pi)^{-1} \int_{\mathbb{R}} \exp\{-iu\tau\} C(\mathbf{h};-u)\, du \\ &= (2\pi)^{-1} \int_{\mathbb{R}} \exp\{iu\tau\} C(\mathbf{h};u)\, du. \end{aligned}$$

If, however, a spatial-temporal process is not stationary in space, then the cross-spectral density function depends not only on distance between arbitrary two stations, but also on their position. The cross-spectral density function in (3.9)

can be also written as

$$f_{\mathbf{ab}}(\tau) = (2\pi)^{-1} \int_{\mathbb{R}} \exp\{-iu\tau\} \mathrm{Cov}\{Z(\mathbf{a}, t), Z(\mathbf{b}, t+u)\}\, du = f^{c}_{\mathbf{ba}}(\tau). \tag{3.10}$$

If a process is axially symmetric in time, that is, $C(\mathbf{h}; u) = C(\mathbf{h}; -u)$, then the cross-spectral density function and the coherency are represented as following:

$$\begin{aligned} f_{\mathbf{ba}}(\tau) &= (2\pi)^{-1} \int_{\mathbb{R}} \exp\{-iu\tau\} C(\mathbf{a}-\mathbf{b}; -u)\, du \\ &= (2\pi)^{-1} \int_{\mathbb{R}} \exp\{-iu\tau\} C(\mathbf{a}-\mathbf{b}; u)\, du = f_{\mathbf{ab}}(\tau). \end{aligned} \tag{3.11}$$

From (3.10) and (3.11), we can easily show that, if the spatial-temporal process Z is axially symmetric in time, then $f_{\mathbf{ab}}(\tau)$ is real-valued. We can also see that, under axial symmetry in time, the phase, $\phi_{\mathbf{ab}}(\tau)$ between $Z(\mathbf{a}; t)$ and $Z(\mathbf{b}; t)$ is represented as follows:

$$\phi_{\mathbf{ab}}(\tau) = \phi_{\mathbf{ba}}(\tau) = 0.$$

Now we propose a new test for lack of axial symmetry in time by using the asymptotic properties of the cross-spectral density function and the phase. For any arbitrary site $\mathbf{a}$, we can define the tapered Fourier transform, $J_{\mathbf{a}}(\tau)$, as

$$J_{\mathbf{a}}(\tau) = \sum_{t=1}^{T-1} K\left(\frac{t}{T}\right) Z\left(\mathbf{a}; t\right) \exp\{-i\tau t\},$$

where K is a tapering function and, in this study, is considered constant, i.e. $K(\mathbf{x}) = 1$ for all $\mathbf{x}$. The spectral window $W(\alpha)$ can be estimated by

$$\widehat{W}(\alpha) = \frac{1}{B_T} \sum_{t=-\infty}^{\infty} W\left(\frac{[\alpha + 2\pi t]}{B_T}\right), \tag{3.12}$$

where B_T is a bandwidth parameter. In the real application, following weight function is considered,

$$\widehat{W}\left(\frac{2\pi s}{T}\right) = \frac{T}{2\pi}(2M+1)^{-1},$$

where $M = B_T T$ and $s \leq M$. We can finally estimate the cross-spectral density function between $Z(\mathbf{a};t)$ and $Z(\mathbf{b};t)$ by

$$\widehat{f}_{\mathbf{ab}}(\tau) = \frac{2\pi}{T}\sum_{t=1}^{T-1}\widehat{W}\left(\tau - \frac{2\pi t}{T}\right)\widehat{I}_{\mathbf{ab}}\left(\frac{2\pi t}{T}\right), \tag{3.13}$$

where the sample cross-periodogram $\widehat{I}_{\mathbf{ab}}(\tau)$ is defined by

$$\widehat{I}_{\mathbf{ab}}(\tau) = \left[2\pi\sum_{t=1}^{T-1}K^2\left(\frac{t}{T}\right)\right]^{-1} J_{\mathbf{a}}(\tau)J^c_{\mathbf{b}}(\tau).$$

Here we introduce some assumptions:

A.1 The weight function $W(\alpha)$ is real-valued, even and of bounded variation such that, for $-\infty < \alpha < \infty$,

$$\int_{\mathbb{R}} W(\alpha)\, d\alpha = 1$$

and

$$\int_{\mathbb{R}} |W(\alpha)|\, d\alpha < \infty.$$

A.2 The temporal covariance is summable, that is, for each $\mathbf{h}$,

$$\sum_{u=-\infty}^{\infty} |u||C(\mathbf{h};u)| < \infty,$$

which implies

$$\sum_{u=-\infty}^{\infty} |C(\mathbf{h}; u)| < \infty$$

and also

A.3 $B_T T \to \infty$ and $B_T \to 0$ as $T \to \infty$.

Under the assumptions **A.1** through **A.3**, the expected value of the estimated cross-spectral density function, $\widehat{f}_{\mathbf{ab}}(\tau)$ can be obtained as

$$\begin{aligned} E\left\{\widehat{f}_{\mathbf{ab}}(\tau)\right\} &= \frac{2\pi}{T}\sum_{t=1}^{T-1} \widehat{W}\left(\tau - \frac{2\pi t}{T}\right) \widetilde{f}_{\mathbf{ab}}(\tau)\left(\frac{2\pi t}{T}\right) + O(T^{-1}) \\ &= \int_{\mathbb{R}} W(\alpha)\widetilde{f}_{\mathbf{ab}}(\tau - B_T\alpha)\, d\alpha + O(B_T^{-1}T^{-1}), \end{aligned}$$

where the error term is uniform in τ, and

$$\widetilde{f}_{\mathbf{ab}}(\tau) = \int_{\mathbb{R}^d} g_\rho(\mathbf{a}-\mathbf{s}) g_\rho(\mathbf{b}-\mathbf{s}) f_{\mathbf{a+s},\mathbf{b+s}}(\tau)\, d\mathbf{s},$$

for $-\infty < \tau < \infty$. Here we consider $\{g_\rho(\mathbf{s})\}$ for $\mathbf{s} = (s_1, s_2)$ to be a tensor product of two one-dimensional filters, $g_\rho(\mathbf{s}) = g_1(s_1)g_2(s_2)$, where g_1 is of the form

$$g_1(s) = 1/\rho \cdot I\{|s| \le \rho/2\},$$

where I is an indicator function. $\widetilde{f}_{\mathbf{ab}}(\tau)$ is the smoothed cross-spectral density function within a band of frequencies in the region of τ and a region in space in the neighborhood of $\mathbf{a}$ and $\mathbf{b}$. And the covariance between $\widehat{f}_{\mathbf{a}_i\mathbf{b}_i}(\tau)$ and $\widehat{f}_{\mathbf{a}_j\mathbf{b}_j}(\lambda)$ is expressed by

$$\begin{aligned} \lim_{T\to\infty} B_T T \mathrm{cov}\left\{\widehat{f}_{\mathbf{a}_i\mathbf{b}_i}(\tau), \widehat{f}_{\mathbf{a}_j\mathbf{b}_j}(\lambda)\right\} &= 2\pi\left(\int_{\mathbb{R}} W^2(\alpha)\, d\alpha\right) \\ \times \left(\eta\{\tau-\lambda\}\left[\widetilde{f}_{\mathbf{a}_i\mathbf{a}_j}(\tau)\widetilde{f}_{\mathbf{b}_i\mathbf{b}_j}(\tau)\right] + \eta\{\tau+\lambda\}\left[\widetilde{f}_{\mathbf{a}_i\mathbf{b}_j}(\tau)\widetilde{f}_{\mathbf{a}_j\mathbf{b}_i}(\tau)\right]\right), \end{aligned} \tag{3.14}$$

where

$$\eta\{\tau\} = \begin{cases} 1 & \text{if } \tau \equiv 0 (\text{mod } 2\pi) \\ 0 & \text{otherwise.} \end{cases}$$

If we define the distance between pairs $(\mathbf{a}_i, \mathbf{b}_i)$ and $(\mathbf{a}_j, \mathbf{b}_j)$ as the minimum distance between any of the two sites in the first pair and any of the two sites in the second pair, then the the estimated cross-spectral density functions, $\widehat{f}_{\mathbf{a}_i\mathbf{b}_i}(\tau)$ and $\widehat{f}_{\mathbf{a}_j\mathbf{b}_j}(\lambda)$, are approximately independent if either

C.1 $\|\tau - \lambda\|$ is sufficiently large so that

$$\int_{\mathbb{R}} |W(\alpha + \tau)|^2 |W(\alpha + \lambda)|^2 \, d\alpha = 0,$$

i.e. if $\|\tau - \lambda\| \gg$ bandwidth of $|W(\alpha)|^2$ or

C.2 the distance between pairs $(\mathbf{a}_i, \mathbf{b}_i)$ and $(\mathbf{a}_j, \mathbf{b}_j)$ is greater than the bandwidth of the function $\{g_\rho(\mathbf{s})\}$.

In practice, we can make the covariance in (3.14) almost zero by having the frequencies τ and λ and the pairs $(\mathbf{a}_i, \mathbf{b}_i)$ and $(\mathbf{a}_j, \mathbf{b}_j)$ sufficiently apart. As mentioned above, the phase is zero in the case of axial symmetry in time. So we can get asymptotic normality of the estimated phase, $\widehat{\phi}_{\mathbf{ab}}(\tau)$, with mean 0 and covariance defined as

$$\begin{aligned} \lim_{T\to\infty} B_T T \, \text{cov}\left\{\widehat{\phi}_{\mathbf{ab}}(\tau), \widehat{\phi}_{\mathbf{ab}}(\lambda)\right\} &= \pi \left(\int_{\mathbb{R}} W^2(\alpha) \, d\alpha\right) \\ &\times \left[\eta\{\tau - \lambda\} - \eta\{\tau + \lambda\}\right] \left[|R_{\mathbf{ab}}(\tau)|^{-2} - 1\right], \end{aligned} \tag{3.15}$$

where the coherency between between $Z(\mathbf{a}; t)$ and $Z(\mathbf{b}; t)$, $R_{\mathbf{ab}}(\tau)$ is defined as

$$R_{\mathbf{ab}}(\tau) = \widetilde{f}_{\mathbf{ab}}(\tau) \Big/ \sqrt{\widetilde{f}_{\mathbf{aa}}(\tau)\widetilde{f}_{\mathbf{bb}}(\tau)}.$$

From (3.15), the asymptotic variance is simply denoted as

$$\lim_{T\to\infty} B_T T \operatorname{Var}\left\{\widehat{\phi}_{\mathbf{ab}}(\tau)\right\} = \pi\left(\int_{\mathbb{R}} W^2(\alpha)\, d\alpha\right)[1-\eta\{2\tau\}]\left[|R_{\mathbf{ab}}(\tau)|^{-2}-1\right]. \tag{3.16}$$

In general, we can not use the asymptotic result of $\widehat{\phi}_{\mathbf{ab}}(\tau)$ for the development of a testing method because the asymptotic variance in (3.16) depends on the relative position of $\mathbf{a}$ and $\mathbf{b}$. So an appropriate transformation is needed. To stabilize the asymptotic variance, we transform $\widehat{\phi}_{\mathbf{ab}}(\tau)$ to $\widetilde{\phi}_{\mathbf{ab}}(\tau)$ given by

$$\widetilde{\phi}_{\mathbf{ab}}(\tau) = \widehat{\phi}_{\mathbf{ab}}(\tau) \Big/ \left[|R_{\mathbf{ab}}(\tau)|^{-2}-1\right]^{1/2}. \tag{3.17}$$

Then we derive the asymptotic normal distribution of $\widetilde{\phi}_{\mathbf{ab}}(\tau)$ with mean 0 and variance given by

$$\begin{aligned}\lim_{T\to\infty} B_T T \operatorname{Var}\left[\widetilde{\phi}_{\mathbf{ab}}(\tau)\right] &= \left[|R_{\mathbf{ab}}(\tau)|^{-2}-1\right]^{-1} \lim_{T\to\infty} B_T T \operatorname{Var}\left\{\widehat{\phi}_{\mathbf{ab}}(\tau)\right\} \\ &= \pi\left(\int_{\mathbb{R}} W^2(\alpha)\, d\alpha\right)[1-\eta\{2\tau\}].\end{aligned}$$

$R_{\mathbf{ab}}(\tau)$ is, however, unknown in practice, so we newly define $\widehat{\phi}^*_{\mathbf{ab}}(\tau)$ as

$$\widehat{\phi}^*_{\mathbf{ab}}(\tau) = \widehat{\phi}_{\mathbf{ab}}(\tau) \Big/ \left[|\widehat{R}_{\mathbf{ab}}(\tau)|^{-2}-1\right]^{1/2}. \tag{3.18}$$

By the Slutsky's theorem, we can obtain the same asymptotic normal distribution of $\widetilde{\phi}_{\mathbf{ab}}(\tau)$ in (3.17) as the one of $\widehat{\phi}^*_{\mathbf{ab}}(\tau)$ in (3.18). Based on the assumptions, **C.1** and **C.2**, we implicitly know that, under the null hypothesis $H_0 : \phi^*_{\mathbf{ab}}(\tau) = \phi_{\mathbf{ab}}(\tau)/\left[|R_{\mathbf{ab}}(\tau)|^{-2}-1\right]^{1/2} = 0$, $\widetilde{\phi}^*$ evaluated at different pairs and different frequencies can be treated independent approximately (see Appendix).

With the information of asymptotic distribution of the adjusted phase, $\widehat{\phi}^*_{\mathbf{ab}}(\tau)$ in (3.18), we propose a formal test for lack of axial symmetry in time by employing analysis of variance (ANOVA) procedure. First we compute $\widehat{\phi}^*_{\mathbf{a}_i\mathbf{b}_i}(\tau_j)$ at arbitrary two sites, $\{(\mathbf{a}_i, \mathbf{b}_i)\}_{i=1}^m$ and a set of temporal frequencies, $\{\tau_j\}_{j=1}^n$ that cover the domain. What is important here is that arbitrary two sites should be selected based on the condition given by

$$\mathbf{a}_i - \mathbf{b}_i = \mathbf{h} = (h_1, h_2, \cdots, h_d)', \quad i = 1, \cdots, m$$

for given $\mathbf{h}$, and the selected pairs of two sites where the distance between the nearest two sites is set greater than the bandwidth of $g_\rho(\mathbf{s})$ in **C.2** in order to make the phase asymptotically independent of each other. In order to apply to two-way ANOVA procedure, we rewrite $\widehat{\phi}^*_{\mathbf{a}_i\mathbf{b}_i}(\tau_j)$ as follows:

$$\widehat{\phi}^*_{\mathbf{a}_i\mathbf{b}_i}(\tau_j) = \phi^*_{\mathbf{a}_i\mathbf{b}_i}(\tau_j) + \epsilon_{\mathbf{a}_i\mathbf{b}_i}(\tau_j), \tag{3.19}$$

where $\phi^*_{\mathbf{a}_i\mathbf{b}_i}(\tau_j) = \phi_{\mathbf{a}_i\mathbf{b}_i}(\tau_j)/\left[|R_{\mathbf{a}_i\mathbf{b}_i}(\tau_j)|^{-2} - 1\right]^{1/2}$. Here $\epsilon_{\mathbf{a}_i\mathbf{b}_i}(\tau_j)$ asymptotically has the following assumptions; $\mathrm{E}\{\epsilon_{\mathbf{a}_i\mathbf{b}_i}(\tau_j)\} = 0,\ \forall i, j$, $\mathrm{Var}\{\epsilon_{\mathbf{a}_i\mathbf{b}_i}(\tau_j)\} = \sigma^2_\epsilon,\ \forall i, j$, and $\mathrm{Cov}\{\epsilon_{\mathbf{a}_i\mathbf{b}_i}(\tau_j), \epsilon_{\mathbf{a}_k\mathbf{b}_k}(\tau_l)\} = 0,\ \forall i, j, k, l$ satisfying **C.1** and **C.2**. We also express (3.19) as

$$\widehat{\phi}^*_{\mathbf{a}_i\mathbf{b}_i}(\tau_j) = \alpha_i + \beta_j + \epsilon_{\mathbf{a}_i\mathbf{b}_i}(\tau_j), \tag{3.20}$$

where the parameters α_i and β_j are spatial location effects and temporal frequency effects, respectively. Suppose that the spatial-temporal process is stationary, then we know that spatial location effect does not depend on the relative position of

the sites, so (3.20) is reduced to

$$\widehat{\phi}^{*}_{\mathbf{a}_i\mathbf{b}_i}(\tau_j) = \beta_j + \epsilon_{\mathbf{a}_i\mathbf{b}_i}(\tau_j), \tag{3.21}$$

If the axial symmetry in time is true under stationarity, then (3.21) can be presented to

$$\widehat{\phi}^{*}_{\mathbf{a}_i\mathbf{b}_i}(\tau_j) = \epsilon_{\mathbf{a}_i\mathbf{b}_i}(\tau_j).$$

So the technique for testing lack of axial symmetry in time under stationarity is just one-way ANOVA with null hypothesis

$$H_0 : \ \beta_j = 0, \quad \forall j = 1, \cdots, n$$

against the alternative hypothesis

$$H_1 : \ \beta_j \neq 0, \quad \exists j = 1, \cdots, n.$$

From (3.20), we can also check the axial symmetry in time as well as the stationarity for the same time by using the two-way ANOVA procedure with the null hypothesis

$$H_0 : \ \alpha_i = 0, \text{ and } \beta_j = 0, \quad \forall i = 1, \cdots, m, \ \forall j = 1, \cdots, n.$$

3.3.2 Test for Lack of Axial Symmetry in Space

Now we talk about the second type of symmetry, axial symmetry in space in Definition 3.3.2. The process is axially symmetric in space provided that the following condition is satisfied:

$$C(\mathbf{h}; u) = C(\mathring{\mathbf{h}}; u),$$

where $\mathring{\mathbf{h}} = (h_1, \cdots, h_{k-1}, -h_k, h_{k+1}, \cdots, h_d)' \neq \mathbf{0}$ for k fixed. For the simplification of developing the test, we only consider $\mathring{\mathbf{h}} = (-h_1, h_2)'$ for $d = 2$. Then we introduce a new version of the cross-spectral density function between $Z(a_1, a_2, t)$ and $Z(a_1, a_2 + h_2, t + u)$, $k(\omega_1, h_2; u)$ given by

$$k(\omega_1, h_2; u) = \int_{\mathbb{R}} \int_{\mathbb{R}} \exp\{ih_2\omega_2 + iu\tau\} g(\boldsymbol{\omega}; \tau)\, d\omega_2\, d\tau, \tag{3.22}$$

for fixed a_2, h_2, t and u. If C is integrable, then

$$\begin{aligned} g(\boldsymbol{\omega}; \tau) &= (2\pi)^{-3} \int_{\mathbb{R}} \int_{\mathbb{R}^2} \exp\{-i\mathbf{h}'\boldsymbol{\omega} - iu\tau\} C(\mathbf{h}; u)\, d\mathbf{h}\, d\tau \\ &= (2\pi)^{-2} \int_{\mathbb{R}} \int_{\mathbb{R}} \exp\{-ih_2\omega_2 - iu\tau\} k(\omega_1, h_2; u)\, du\, dh_2. \end{aligned}$$

Since the function k in (3.22) is the Fourier transform of the spatial-temporal covariance function with respect to one of the spatial frequencies, we can also write k in an alternative form denoted by

$$k(\omega_1, h_2; u) = (2\pi)^{-1} \int_{\mathbb{R}} \exp\{-ih_1\omega_1\} C(h_1, h_2; u)\, dh_1.$$

If a process is axially symmetric in space, that is, $C(h_1, h_2; u) = C(-h_1, h_2; u)$, then

$$\begin{aligned} k(\omega_1, h_2; u) &= (2\pi)^{-1} \int_{\mathbb{R}} \exp\{-ih_1\omega_1\} C(h_1, h_2; u)\, dh_1 \\ &= (2\pi)^{-1} \int_{\mathbb{R}} \exp\{-ih_1\omega_1\} C(h_1, -h_2; u)\, dh_1 = k(-\omega_1 h_2; u) \\ &= (2\pi)^{-1} \int_{\mathbb{R}} \exp\{ih_1\omega_1\} C(h_1, h_2; u)\, dh_1. \end{aligned}$$

So, in case of the axial symmetry in space, the following condition is always satisfied:

$$\begin{aligned} & k(\omega_1,h_2;u) - k(\omega_1,h_2;u) \\ & \quad = (2\pi)^{-1} \int_{\mathbb{R}} \left[\exp\{ih_1\omega_1\} - \exp\{-ih_1\omega_1\}\right] C(h_1,h_2;u)\, dh_1 \\ & \quad = \frac{i}{\pi} \int_{\mathbb{R}} \sin(h_1\omega_1) C(h_1,h_2;u)\, dh_1 = 0. \end{aligned} \tag{3.23}$$

From (3.23), we know that, if the spatial-temporal process Z is axially symmetric in space, then the function, k is always real-valued. So we can get the following result:

$$\begin{aligned} \psi(\omega_1;h_2,u) &= \tan^{-1}\left\{\frac{\text{Im.}k(\omega_1,h_2;u)}{\text{Re.}k(\omega_1,h_2;u)}\right\} = \tan^{-1}\left\{\frac{\text{Im.}k(-\omega_1,h_2;u)}{\text{Re.}k(-\omega_1,h_2;u)}\right\} \\ &= \psi(-\omega_1;h_2,u) = 0, \end{aligned}$$

where $\psi(\omega_1;h_2,u)$ is a new version of the phase between $Z(a_1,a_2,t)$ and $Z(b_1,a_2+h_2,t+u)$ for fixed a_2, h_2, t and u.

Now we propose a new testing method for the asymptotic properties of the functions k and ψ. If Z is observed only at $N(=N_1N_2)$ sites on regular grids and at the measuring times T, then, for a_2 and t fixed, we can define $J_{\Delta_1}(\omega_1;a_2,t)$,

$$J_{\Delta_1}(\omega_1;a_2,t) = \Delta_1 \sum_{n_1=1}^{N_1-1} K\left(\frac{n_1}{N_1}\right) Z\left(\Delta_1 n_1, a_2; t\right) \exp\left\{-i\Delta_1 n_1 \omega_1\right\},$$

where Δ_1 is the unit distance of the first spatial coordinate. We also define the sample spectral window $\widehat{W}(\alpha)$ by

$$\widehat{W}(\alpha) = \frac{1}{B_{N_1}} \sum_{j=-\infty}^{\infty} W\left(\frac{[\alpha+2\pi j]}{B_{N_1}}\right), \tag{3.24}$$

where $-\infty < \alpha < \infty$. Then $\widehat{k}_{\Delta_1}(\omega_1, h_2; u)$ is represented by

$$\widehat{k}_{\Delta_1}(\omega_1, h_2; u) = \frac{2\pi}{N_1} \sum_{n_1=1}^{N_1-1} \widehat{W}\left(\omega_1 - \frac{2\pi n_1}{N_1}\right) \widehat{I}_{\Delta_1}\left(\frac{2\pi n_1}{N_1}; h_2, u\right), \tag{3.25}$$

where

$$\widehat{I}_{\Delta_1}(\omega_1; h_2, u) = \left[2\pi \sum_{n_1=1}^{N_1-1} \left\{K^2\left(\frac{n_1}{N_1}\right)\Delta_1\right\}\right]^{-1} \times J_{\Delta_1}(\omega_1; a_2, t)\, J^c_{\Delta_1}(\omega_1; a_2 + h_2, t + u).$$

Here we introduce some additional assumptions:

A.4 The spatial covariance is summable, that is, for fixed h_2 and u,

$$\int_{\mathbb{R}} |h_1||C(h_1, h_2; u)|\, dh_1 < \infty,$$

which also implies

$$\int_{\mathbb{R}} |C(h_1, h_2; u)|\, dh_1 < \infty.$$

A.5 $B_{N_1} N_1 \to \infty$ and $B_{N_1} \to 0$ as $N_1 \to \infty$.

Under the assumptions **A.1**, **A.4** and **A.5**, we can obtain the asymptotic properties of the esimated phase, $\widehat{\psi}_{\Delta_1}(\omega_1; h_2, u)$ with mean $\psi_{\Delta_1}(\omega_1; h_2, u)$ and the variance defined as

$$\begin{aligned} &\lim_{N_2 \to \infty} B_{N_1} N_1 \mathrm{Var}\left\{\widehat{\psi}_{\Delta_1}(\omega_1; h_2, u)\right\} \\ &\quad = \pi \left(\int_{\mathbb{R}} W^2(\alpha)\, d\alpha\right) [1 - \eta\{2\omega_1\}] \left[|Q_{\Delta_1}(\omega_1; h_2, u)|^{-2} - 1\right], \end{aligned} \tag{3.26}$$

where a new version of the coherency, $Q(\omega_1; h_2, u)$ between two arbitrary points in two-dimensional space, (a_2, t) and $(a_2 + h_2, t + u)$, is defined by

$$Q(\omega_1; h_2, u) = k(\omega_1, h_2; u) \Big/ |k(\omega_1, 0; 0)|.$$

Here a_2 is the second spatial coordinate of a site $\mathbf{a}$ and t is a measure of time. In general, we can not directly use the asymptotic result of $\widehat{\psi}_{\Delta_1}(\omega_1; h_2, u)$ in order to make a new test for lack axial symmetry in space because the asymptotic variance in (3.26) depends on h_2 and u. In order to make the asymptotic variance independent of h_2 and u we transform $\widehat{\psi}_{\Delta_1}(\omega_1; h_2, u)$ to $\widetilde{\psi}_{\Delta_1}(\omega_1; h_2, u)$ defined by

$$\widetilde{\psi}_{\Delta_1}(\omega_1; h_2, u) = \widehat{\psi}_{\Delta_1}(\omega_1; h_2, u) \Big/ \left[|Q_{\Delta_1}(\omega_1; h_2, u)|^{-2} - 1\right]^{1/2}. \tag{3.27}$$

In practice, however, $Q_{\Delta_1}(\omega_1; h_2, u)$ is a unknown parameter, so, by using the estimated coherency, $\widehat{Q}_{\Delta_1}(\omega_1; h_2, u)$, we newly define $\widehat{\psi}^*_{\Delta_1}(\omega_1; h_2, u)$ as

$$\widehat{\psi}^*_{\Delta_1}(\omega_1; h_2, u) = \widehat{\psi}_{\Delta_1}(\omega_1; h_2, u) \Big/ \left[|\widehat{Q}_{\Delta_1}(\omega_1; h_2, u)|^{-2} - 1\right]^{1/2}. \tag{3.28}$$

If we use an appropriate $\widehat{Q}_{\Delta_1}(\omega_1; h_2, u)$ as an estimate of $Q_{\Delta_1}(\omega_1; h_2, u)$, then we can get the same asymptotic distribution of $\widehat{\psi}^*_{\Delta_1}(\omega_1; h_2, u)$ in (3.28) as the one of $\widetilde{\psi}_{\Delta_1}(\omega_1; h_2, u)$ in (3.27).

Now we propose a formal test for axial symmetry in space for spatial-temporal processes. For the m pairs, $\left\{\left(a_2^i, t_i^a; b_2^i, t_i^b\right)\right\}_{i=1}^m$, in two-dimensional space consisting of the second spatial and the temporal coordinates, and a set of first spatial frequencies, $\{\omega_j\}_{j=1}^n$, we can get $\widehat{\psi}^\star_i(\omega_j) \equiv \widehat{\psi}^*_{\Delta_1}\left(\omega_j; (a_2^i, t_i^a; b_2^i, t_i^b)\right)$. Arbitrarily, the pairs of two points in two-dimensional space are selected based on the conditions

given by

$$a_2^i - b_2^i = h_2, \quad \text{and} \quad t_i^a - t_i^b = t_i^c - t_i^d = u,$$

for $i = 1, \cdots, m$ and for the given first spatial lag h_2 and time lag u. It is important for the minimum distance between arbitrary two pairs to be larger than the bandwidth, $g_\rho(\mathbf{s})$ in order for $\widehat{\psi}_i^\star(\omega_j)$ to be asymptotically independent. In order to apply to traditional two-way ANOVA procedure, we rewrite $\widehat{\psi}_i^\star(\omega_j)$ as follows:

$$\widehat{\psi}_i^\star(\omega_j) = \psi_i^\star(\omega_j) + e_i(\omega_j), \tag{3.29}$$

where

$$\psi_i^\star(\omega_j) = \psi_{\Delta_1}\left(\omega_j; (a_2^i, t_i^a; b_2^i, t_i^b)\right) \Big/ \left[\left| Q_{\Delta_1}\left(\omega_j; (a_2^i, t_i^a; b_2^i, t_i^b)\right)\right|^{-2} - 1\right]^{1/2},$$

$\mathrm{E}\{e_i(\omega_j)\} = 0$ and $\mathrm{Var}\{e_i(\omega_j)\} = \sigma_e^2$, asymptotically, and $\mathrm{Cov}\{e_i(\omega_j), e_k(\omega_l)\} = 0$, $\forall i, j, k, l$ approximately. We also express (3.29) as

$$\widehat{\psi}_i^\star(\omega_j) = \gamma_i + \delta_j + e_i(\omega_j), \tag{3.30}$$

where the parameters γ_i and δ_j are the space-time interaction and the spatial frequency effect, respectively. Since we know that, under the stationarity, the covariance between any two measurements is not dependent on their relative postion, it is quite reasonable to assume that the space-time interaction effect, γ_i, is equal to 0. So, under stationarity, (3.30) is reduced to

$$\widehat{\psi}_i^\star(\omega_j) = \delta_j + e_i(\omega_j). \tag{3.31}$$

If axial symmetry in space holds under stationarity, then (3.31) is presented by

$$\widehat{\psi}_i^{\star}(\omega_j) = e_i(\omega_j).$$

From (3.31), we can easily construct a new test for axial symmetry in space under stationarity by applying to the one-way ANOVA technique with the null hypothesis

$$H_0 : \ \delta_j = 0, \quad \forall j = 1, \cdots, n$$

against the alternative hypothesis

$$H_1 : \ \delta_j \neq 0, \quad \exists j = 1, \cdots, n.$$

From (3.30), we can also check the space-time interaction effect if we consider the one-way ANOVA structure with the null hypothesis

$$H_0 : \ \gamma_i = 0, \quad \forall i = 1, \cdots, m$$

against the alternative hypothesis

$$H_0 : \ \gamma_i \neq 0, \quad \exists i = 1, \cdots, m.$$

3.4 Simulation Study

In Section 3.3, we proposed new formal tests for lack of axial symmetry in time and lack of axial symmetry in space in spatial-temporal processes. In this section, we evaluate the performance of these tests by simulation study where the

underlying covariance is an asymmetric exponential stationary spatial-temporal one. Now we introduce the simulation steps for checking the behaviours of the new tests. Here we examine the case for the axial symmetry in time.

1) Find m pairs of sites which are far from each other as specified by the spatial lags, $\mathbf{h} = (h_1, h_2)'$. Keep the minimum spatial distance between the nearest two sites in arbitrary two pairs greater than the bandwidth of $g_\rho(\mathbf{s})$ in **C.2** to make their processes asymptotically independent.

2) Compute the test statistic shown in (3.18) for each pair.

3) Apply this setup to the traditional ANOVA procedure by considering the calculated value, temporal frequency, spatial direction, and subregion including a pair.

In case of axial symmetry in space, one of the major differences from the previous case occurs in step 1). The steps for testing the axial symmetry in space are as follow:

1) Find m pairs of points which are far from each other as specified by the second spatial lag (latitudinal lag) and the temporal lag, $(h_2, u)'$. Keep the minimum distance between the nearest two points in arbitrary two pairs larger than or equal to the spatial and the temporal ranges enough to make their processes asymptotically independent.

2) Compute the test statistic proposed in (3.28) for each pair.

3) Apply this setup to the traditional ANOVA procedure by considering the calculated value, first spatial frequency, and subregion including a pair..

For the simplification of the simulation setup, we consider the spatial bandwidth $g_\rho(\mathbf{0})$, that is, we only focus on the cross spectral density functions at the selected pairs.

Before presenting the simulation study, we briefly explain the asymmetric spatial-temporal covariance given by

$$C(\mathbf{h}; u) = \sigma_1 \exp\left\{-\sqrt{\beta^2(u - \mathbf{h}'\mathbf{v})^2 + \alpha^2\|\mathbf{h}\|^2}\right\} + \sigma_0 I(\|\mathbf{h}\| = u = 0), \qquad (3.32)$$

where σ_0 is the nugget, σ_1 is the partial sill, α is the decaying rate of spatial correlation, β is the decaying rate of temporal correlation, and $\mathbf{v} \in \mathbb{R}^2$ is the asymmetry parameter vector. This vector, $\mathbf{v} = (v_1, v_2)'$ controls the types of asymmetry realized in spatial-temporal processes. For example, $\mathbf{v} = \mathbf{0}$ yields the covariance satisfying axial symmetry in time. If only one element in $\mathbf{v}$ is zero, then axial symmetry in space is satisfied. Diagonal symmetry in space is called in case that $v_1 = v_2 \neq 0$. We call asymmetry in space and time, otherwise.

Now we explain the fundamental simulation setup for realizing the tests for lack of symmetry. The number of iterations is set to 100 and, at each iteration, the observations are generated from the multivariate normal distribution with the mean 0 and the variance-covariance matrix extended from (3.32). The covariance parameters are preassigned as follows; $\sigma_0 = 0.01$, $\sigma_1 = 1$, $\alpha = 0.02$, $\beta = 0.75$. Here the spacing unit for locations is 10 and the unit for time is 1.

3.4.1 Testing Lack of Axial Symmetry in Time

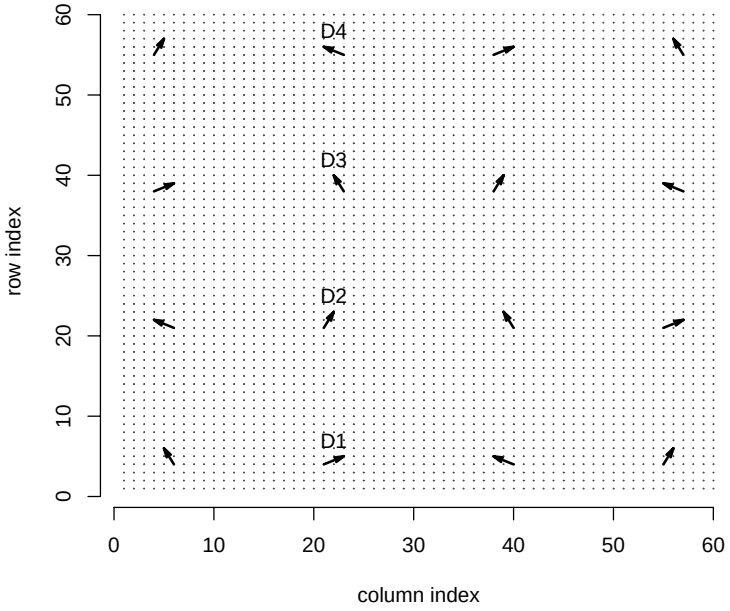

Figure 3.1: Selection of Pairs for the Test for Lack of Axial symmetry in Time. Note that we consider four different directions in spatial domain; ENE (D1), NNE (D2), NNW (D3), and WNW (D4).

For the test for lack of axial symmetry in time, we consider the spatial domain with 16 pairs of two sites as shown in Figure 3.1 and we generate 51 observations over time at each selected site. The spatial distance between any pairs is set to as much as or greater than the effective spatial range, $3/\alpha = 15$. The temporal frequencies, τ_j are selected as follows; $\tau_j = \pi j/25$ with $j = 3$ (5) 23. We then construct the test statistic for lack of axial symmetry in time, $\widehat{\phi}^{*}_{\mathbf{a}_i\mathbf{b}_i}(\tau_j)$ in (3.20) at the following temporal frequencies; $3\pi/25$, $8\pi/25$, $13\pi/25$, $\cdots$, $23\pi/25$. As can be seen in Figure 3.1, we also consider four different directions as well as 16 subregions in spatial domain.

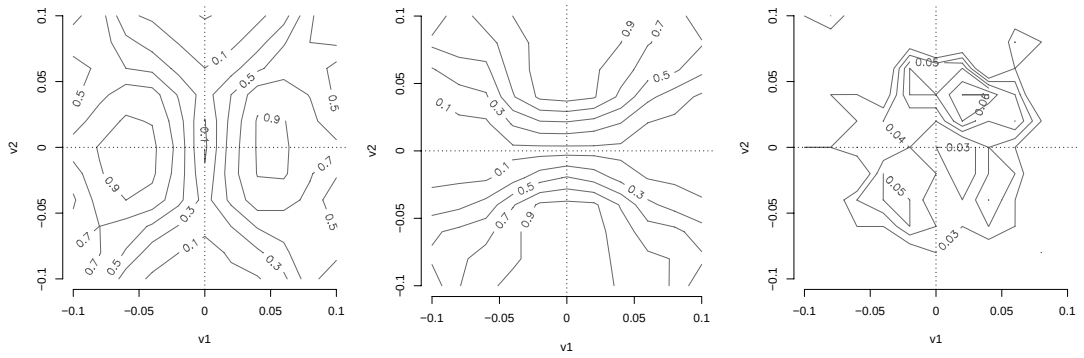

(a) (b) (c)

Figure 3.2: The Contour Plots of Empirical Powers Under General Asymmetry in Space and Time for Main Effects from ANOVA Technique. Note that the dotted lines are about axial symmetry in space and the dashed line is for diagonal symmetry in space, and the null hypothesis is located on the origin ($\mathbf{v} = \mathbf{0}$). (a) Empirical powers for the effect of "Direction"; (b) empirical powers for the effect of "Temporal Frequency"; (c) empirical powers for the effect of "Subregion".

Figure 3.2 displays the contour plots of empirical powers for the main effects of "Direction" and of "Temporal Frequency" under asymmetry in space and time, that is, under $\mathbf{v} \neq 0$. Figure 3.2 (a) confirms that the nonzero temporal frequency in terms of the directions is well detected in case that $v_1 \neq 0$ but $v_2 = 0$ (the horizontal dotted line) rather than in case that $v_1 = 0$ but $v_2 \neq 0$ (the vertical dotted line) although these two dotted lines mean the same alternative hypothesis, axial symmetry in space. The reason is that all the directions we considered are roughly in north direction not E-W direction. However, Figure 3.2 (b) shows the opposite performance of the effect of "Direction". Detecting Lack of axial symmetry in time is much better under the siutation where $v_1 = 0$ but $v_2 \neq 0$. So, there exists some complementary relationship between direction in spatial domain and temporal frequency. Here, if we are interested in the alternative

hypothesis, axial symmetry in space where $v_1 = 0$ but $v_2 \neq 0$ (the vertical dotted line), the performance of the test statistic is almost perfect. In addition, from the low empirical powers of the effect of "Subregion" in Figure 3.2 (c), informs us that lack of stationarity is rarely detected, which is a reasonable result because the spatial-temporal covariance function used in this simulation study is stationary.

Table 3.1: Empirical Powers of an Alternative Hypothesis that $v_1 = 0$ but $v_2 \neq 0$. Note that the situation that $v_1 = 0$ but $v_2 \neq 0$ is the vertical dotted line in each plot of Figure 3.2.

Main Effects	v_2								
	-.08	-.06	-.04	-.02	0.00	0.02	0.04	0.06	0.08
Locations	0.03	0.04	0.03	0.04	0.03	0.03	0.06	0.05	0.00
Directions	0.02	0.15	0.22	0.13	0.06	0.09	0.21	0.10	0.03
Frequencies	0.99	1.00	0.96	0.52	0.02	0.46	0.98	0.98	0.93

Table 3.1 shows the empirical powers under one of the alternative hypotheses, that is, in case that $v_1 = 0$ but $v_2 \neq 0$. We see that, from the effect of temporal frequencies, lack of axial symmtry in time is well detected even when v_2 slightly moves from 0 and there is not any big difference of powers in terms of the direction.

3.4.2 Testing Lack of Axial Symmetry in Space

What we have to consider next is to check whether lack of axial symmetry in space, $C(h_1, h_2; u) \neq C(-h_1, h_2; u)$ is in the spatial-temporal process or not. For testing lack of axial symmetry in space, we consider 16 pairs of two points where the position of each point is represented by a spatial index and a time

index (Figure 3.3). The spatial frequencies, ω_j are selected as follows; $\omega_j =$

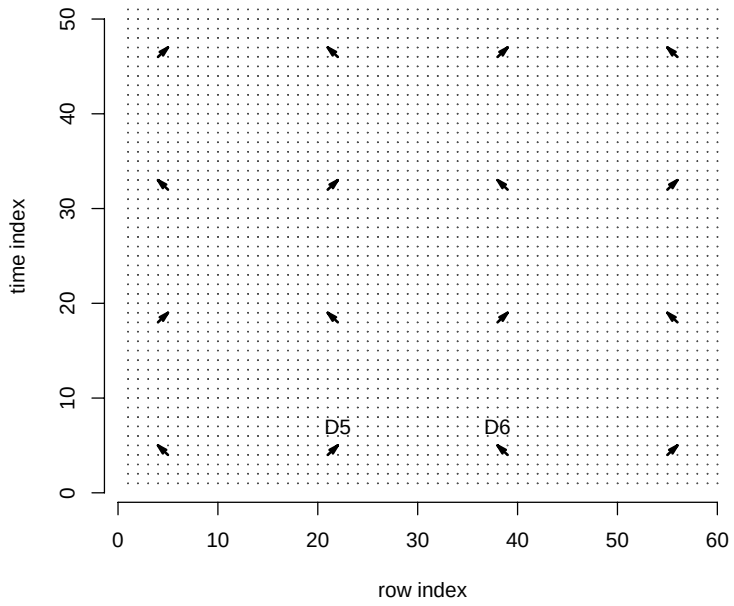

Figure 3.3: Selection of Pairs for the Test for Lack of Axial symmetry in Space. Note that we consider the two different directions in two dimensional (spatial-temporal) domain; D5 and D6.

$\pi j/30$ with $j = 2$ (9) 29. We then construct the test statistic for lack of axial symmetry in space, $\widehat{\psi}_i^{\star}(\omega_j)$ in (3.31) at the following spatial frequencies; $2\pi/30$, $11\pi/30$, $20\pi/30$, and $29\pi/30$. Figure 3.3 also shows that four different directions as well as 16 subregions defined in two dimensional domain, which consists of one dimensional spatial domain and a temporal domain, are considered. The reason why the directions are taken into account is that we want to check spatial-temporal interaction.

Now we explain the results obtained from the ANOVA approach including the three effects; "Direction", "Subregion", and "Spatial Frequency". Figure 3.4

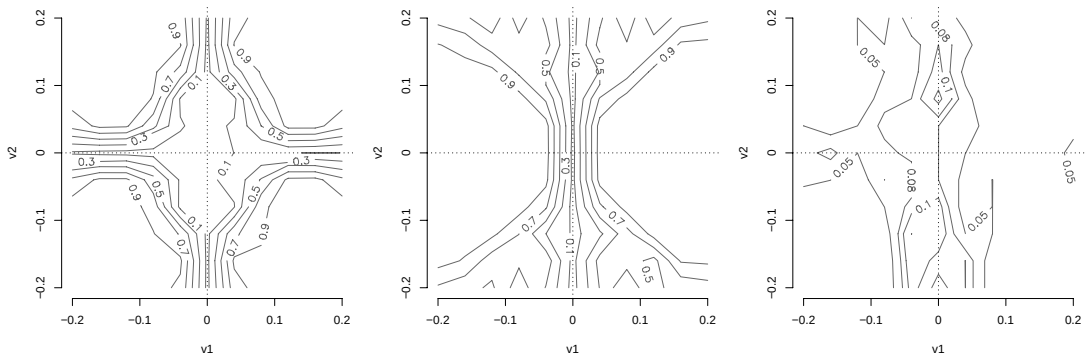

(a) (b) (c)

Figure 3.4: The Contour Plots of Empirical Powers Under General Asymmetry in Space and Time for Main Effects from ANOVA Technique. Note that the vertical dotted line is the null hypothesis, axial symmetry in space ($v_1 = 0$, $v_2 \neq 0$). (a) Empirical powers for the effect of "Direction"; (b) empirical powers for the effect of "Spatial Frequency"; (c) empirical powers for the effect of "Subregion".

displays the empirical power for each main effect under general asymmetry in space and time with $\mathbf{v} \neq \mathbf{0}$. From Figure 3.4 (a), we see that, in case of the effect of "Direction", the empirical powers under the null hypothesis are well maintained and nonzero spatial frequency is detected under the situation where $v_1 \neq 0$ and $v_2 \neq 0$. We can also know that, from Figure 3.4 (b), the performance of the test is only explained well in that the power increases as v_1 goes far from 0 only if $-0.5 < v_2 < 0.5$. Figure 3.4 (c) informs that there seems no big difference of spatial frequencies among the the positions of two points in spatial-temporal domain. This is quite related to the existence of stationarity.

Figure 3.4(a) and (b) confirm that the test for lack of axial symmetry in space really depends on how the directions are assigned in the spatial-temporal domain. So we need focus on the behaviour of spatial frequencies in terms of each direction

shown in Figure 3.3. Since lack of stationarity is not detected for all $\mathbf{v}$ we now

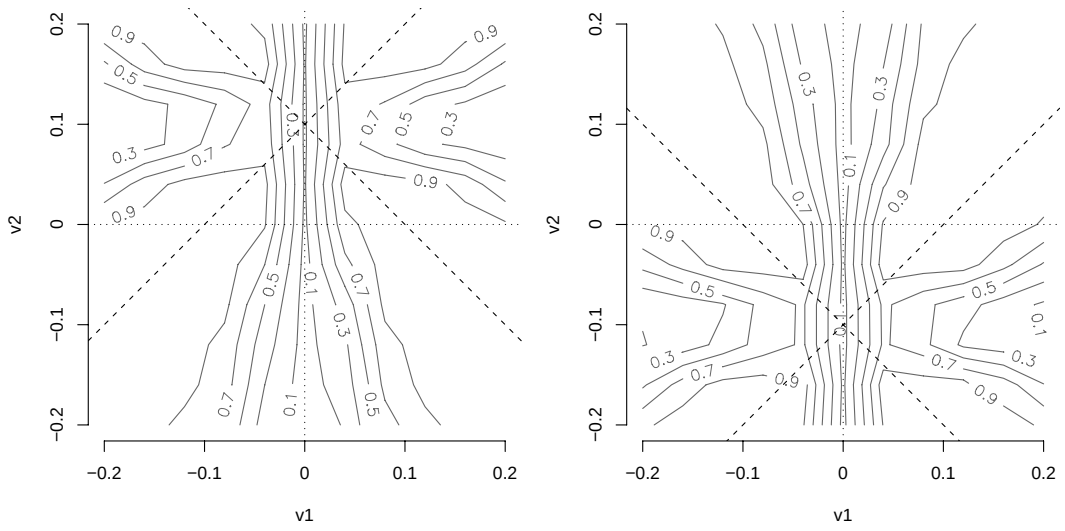

(a) (b)

Figure 3.5: The Contour Plots of Empirical Powers Under General Asymmetry in Space and Time for the "Spatial Frequency" Effect from ANOVA Technique in terms of each direction. (a) Empirical powers under the direction, D5; (b) empirical powers under the direction, D6.

consider the ANOVA model with just the effect of "Spatial Frequency" for each direction. From Figure 3.5(a) and (b), we can see that the actual null hypotheses are located on $\mathbf{v} = (0, 0.1)'$ for D5 and on $\mathbf{v} = c(0, -0.1)'$ for D6. The reason is that these two combinations are the solutions of $u - \mathbf{h}'\mathbf{v} = 0$. For example, the spatial and temporal lags between two points on the direction, D5 are $h_2 = -10$ and $u = -1$, and then $u - \mathbf{h}'\mathbf{v} = 0$. What is interesting here is that the empirical power increases as $\mathbf{v}$ goes far from the correponding null hypothesis along the dashed lines, which is quite related to what the direction is considered.

Table 3.2 displays the empirical powers under the alternative hypotheses shown

Table 3.2: Empirical Powers of an Alternative Hypothesis meaning the dashed lines in the plots of Figure 3.5.

	$\mathbf{v} = (v_1, v_2)'$								
v_1	-.20	-.16	-.12	-.08	-.04	0.00	0.04	0.08	0.12
v_2	-.12	-.08	-.04	0.00	0.04	0.08	0.12	0.16	0.20
Frequencies	1.00	1.00	1.00	1.00	1.00	0.04	0.73	1.00	1.00
v_1	-.20	-.16	-.12	-.08	-.04	0.00	0.04	0.08	0.12
v_2	0.12	0.08	0.04	0.00	-.04	-.08	-.12	-.16	-.20
Frequencies	1.00	1.00	1.00	1.00	0.96	0.07	0.83	1.00	1.00

in Figure 3.5 (the dashed lines). As one can see, lack of axial symmtry in space is well detected even when $\mathbf{v}$ slightly moves from $\mathbf{v} = (0, -0.1)'$ or $\mathbf{v} = c(0, 0.1)'$.

We have presented the simulation results of the two tests for lack of symmetry in spatial-temporal processes so far. Both of the tests performs well in terms of the empirical powers. However, each test depends on how the directions are considered.

3.5 Real Application

In Section 3.4, we evaluated the performances of the two tests for lack of symmetry proposed in Section 3. As the results from the simulation study, the tests detect the corresponding lack of symmetry under general situation with asymmetry in space and time. In this section, we apply the new testing methods

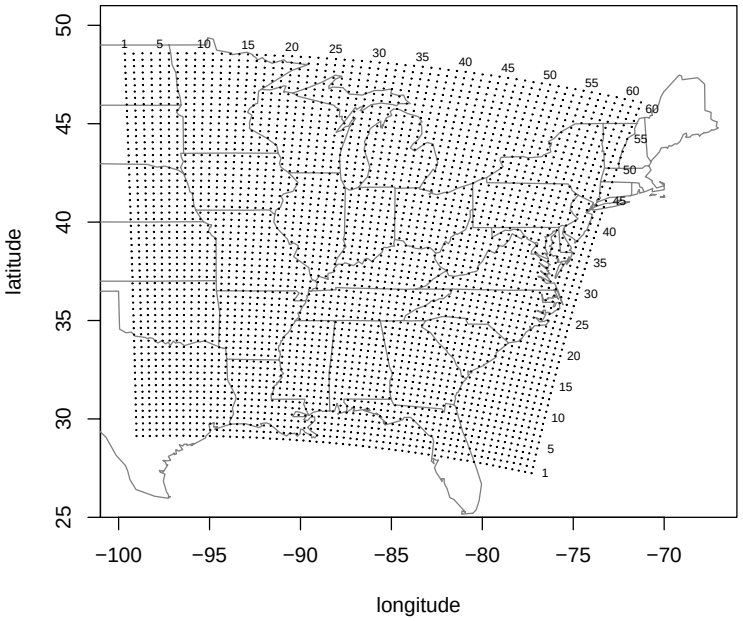

Figure 3.6: The map of the locations of 3721 ($= 61 \times 61$) centroids of grid cells where each cell is size of $36km \times 36km$. Note that the numbers on the right of grid cells are row indice and the ones on the top are column indice.

to the real air-pollution dataset. Here we consider the daily $PM_{2.5}$ concentrations which were the averages of hourly values, which are obtained from the Models-3/Community Multiscale Air Quality (CMAQ) modeling system with the spatial resolution of $36km \times 36km$. These data were provided by the U.S EPA The spatial domain of our interest is the eastern U.S and the southern Canada, and the time domain is January 1st through December 29th, 2001. The main reason why we are interested in $PM_{2.5}$ concentrations is that this air-pollutant is one of the important factors in the public health problem and, according to many environmenal studies, has complex spatial or spatial-temporal dependency structure (Zidek (1997) and Golam Kibria *et al.* (2002)).

Before applying the test for lack of axial symmetry in time, we remove the spatial and the temporal trends. For a $PM_{2.5}$ concentration at location $\mathbf{s}$ and time t, $Z(\mathbf{s}, t)$, we remove the average over time at each location and the average over space at each time. Then we employ our tests for lack of symmetry to the $PM_{2.5}$ anomaly concentrations subtracted by the spatial and temporal trends. Here the spatial bandwidth $g_\rho(\mathbf{0})$ is considered for the simplicity for analyzing the data.

3.5.1 Testing Lack of Axial Symmetry in Time

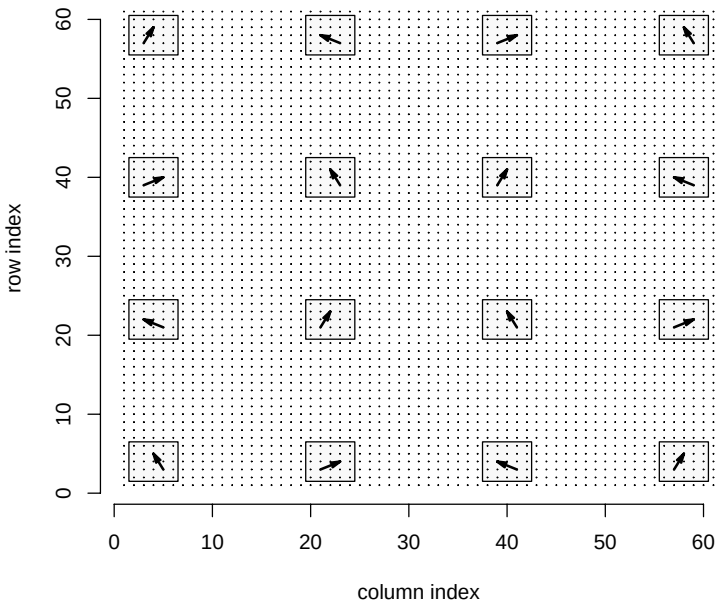

Figure 3.7: The plot of the locations of the selected 16 pairs. Note that four different directions are considered; ENE direction (D1), NNE direction (D2), NNW direction (D3), and WNW (D4).

We obtain the estimates of phase and coherency, $\widehat{\phi}_{\mathbf{ab}}(\tau)$ and $\widehat{R}_{\mathbf{ab}}(\tau)$ by calcu-

lating the estimated cross-spectrum in (3.13) where the spectral window, $\widehat{W}(\alpha)$ in (3.12) has a bandwidth of $2\pi B_T$ with $B_T = 1/28$. In order to make the estimates uncorrelated approximately, we choose the temporal frequencies τ_j for $j = 1, \cdots, n = \lfloor B_T T \rfloor$ satisfying that the spacings between the τ_j are at least $\pi/14$, the distance between any pairs, $(\mathbf{a}_i, \mathbf{b}_i)$ and $(\mathbf{a}_j, \mathbf{b}_j)$ for $i \neq j$ is set larger than or equal to the spatial range, $1/\alpha$ and the distance within any pair is also set much smaller than the spatial range. Here $\lfloor a \rfloor$ means the integer nearest to a.

The temporal frequencies, τ_j are selected as follows; $\tau_j = \pi j/181$ with $j = 6$ (13) 175, where the uniform spacing of $13\pi/181$ is slightly longer than $\pi/14$. We then construct the test statistic, for lack of axial symmetry in time, $\widehat{\phi}^*_{\mathbf{a}_i\mathbf{b}_i}(\tau_j)$ in (3.20) at the following temporal frequencies; $\tau_1 = 6\pi/181$, $\tau_2 = 19\pi/181, \cdots$, $\tau_{13} = 175\pi/181$. We consider the 16 pairs, $\{\mathbf{a}_i, \mathbf{b}_i\}$, $i = 1, \cdots, 16$ shown in Figure 3.7. It can be seen, from Figure 3.7, that the spatial distance between pairs is at least 13 spacing units (unit=$36km$) and the distance within each pair is set to $\sqrt{5}$ units. We also take into account the effect of the directions decided by two locations consisting of each pair.

Table 3.3: Analysis of variance

Item	Degree of freedom	Sum of squares	F value	Pr(F)
Directions	4	1.6028	15.9463	0.0000
Locations	12	0.9811	3.2537	0.0003
Frequencies	12	0.1681	0.5576	0.8736
Residuals	180	4.5229		

Table 3.3 shows the result of the test for lack of axial symmetry in time. The effect of "temporal frequency" is not significant under 5% significance level, so it is clear evidence of axial symmetry in time, that is, $C(h_1, h_2; u) = C(h_1, h_2; -u)$. However, the other main effets, "Locations" (p-value< 0.0000) and "Directions" (p-value< 0.001) are statistically significant. Thus, there exists nonstationarity, which might influence the effect of "Directions". Here we investigate existence of lack of axial symmetry in time more in detail in terms of directions in order to understand how much contribution each direction has.

Table 3.5 displays the result from two-way ANOVA technique for each direction given. We can see that for most of the directions, nonstationarity problem exists except NNW direction (D3), but lack of axial symmetry in time exists in case of ENE direction (D1) and WNW direction (D4). This phenomenon implies that the flow of the external conditions such as wind direction might be in E-W direction or W-E direction.

Figure 3.8 shows QQplots to check whether the residuals from the ANOVA in Table 3.5 have lack of normality. We can conclude that the deviation of the residuals from normality does not seem to be serious for either case of directions. The p-values calculated from the Kolmogorov-Smirnov normality test are 0.27 and 0.28, respectively.

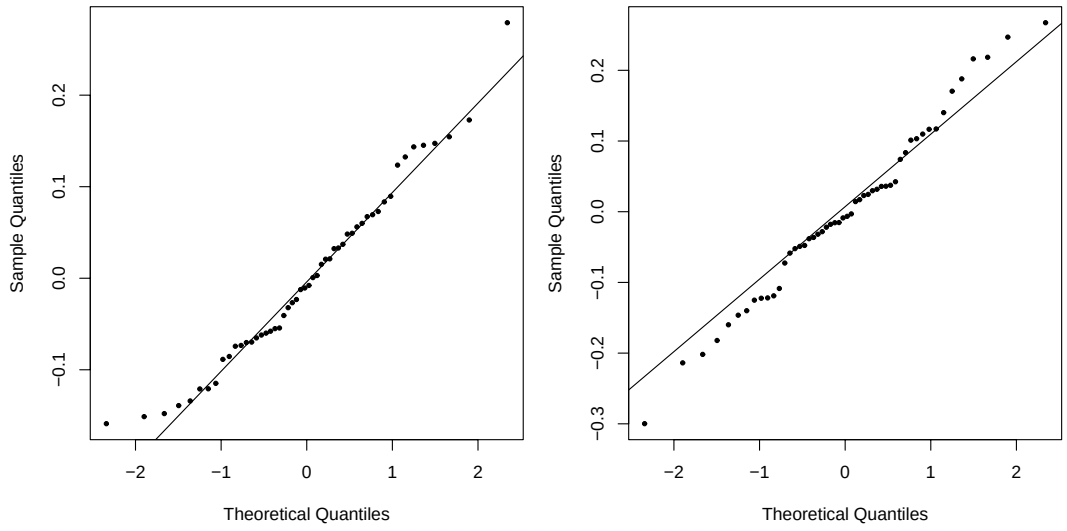

(a) (b)

Figure 3.8: The QQplots of the residuals (a) The quantiles from $N(0,1)$ versus the residuals in case of ENE direction (D1); (b) the quantiles from $N(0,1)$ versus the residuals in case of WNW direction (D4).

3.5.2 Testing Lack of Axial Symmetry in Space

In order to obtain the estimates of phase and coherency, $\widehat{\psi}_{\Delta_1}$ and $\widehat{Q}_{\Delta_1}$ in (3.28), we estimate the new version of cross-spectrum in (3.25) where the spectral window, $\widehat{W}(\alpha)$ in (3.24) has a bandwidth of $2\pi B_{N_1}$ with $B_{N_1} = 1/12$. In order to make the estimates uncorrelated approximately, we choose the temporal frequencies ω_j for $j = 1, \cdots, n = \lfloor B_{N_1} N_1 \rfloor$ satisfying that the spacings between the ω_j are at least $\pi/6$, the distance between any pairs, $\{(a_2^i, t_i^a), (b_2^i, t_i^b)\}$ and $\{(a_2^j, t_j^a), (b_2^j, t_j^b)\}$ for $i \neq j$ is set larger than or equal to the spatial range as well as the temporal range, $1/\beta$ and the distance within each pair, for example, $\sqrt{(a_2^i - b_2^i)^2 + (t_i^a - t_i^b)^2}$ for i_{th} pair, is set much smaller than the spatial and the temporal ranges.

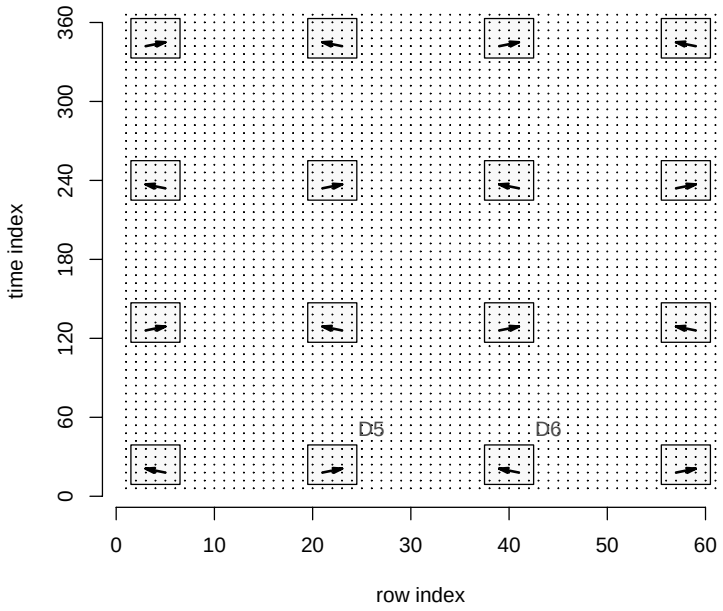

Figure 3.9: The plot of the locations of the selected 16 pairs. Note that two directions are considered; D5, D6.

We consider the following spatial frequencies, ω_j; $\omega_j = \pi j/10$ with $j = 1\ (2)\ 9$, where the uniform spacing of $\pi/5$ is slightly longer than $\pi/6$. The test statistic for lack of axial symmetry in space, $\widehat{\psi}_i^{\star}(\omega_j)$ in (3.29) is constructed at the following temporal frequencies; $\omega_1 = \pi/10$, $\omega_2 = 3\pi/10$, $\cdots$, $\omega_5 = 9\pi/10$. We consider the 16 pairs, $\{(a_2^i, t_i^a),\ (b_2^i, t_i^b)\}$, $i = 1, \cdots, 16$ shown in Figure 3.9. It can be seen, from Figure 3.9, that the minimum temporal distance between pairs is at least 100 units (unit=1 day) and the minimum spatial distance in terms of column index is more than 15 units (unit=$36km$). The distance within each pair is set to $\sqrt{1^2\text{day}^2 + 72^2 km^2}$. The effect of the directions decided by two locations consisting of each pair is also taken into account.

Table 3.4 displays the result of the test for lack of axial symmetry in space.

Table 3.4: Analysis of variance

Item	Degree of freedom	Sum of squares	F value	$\Pr(F)$
Directions	2	0.0263	0.0273	0.9730
Interactions	14	4.8976	0.7262	0.7400
Frequencies	4	6.6600	3.4564	0.0132
Residuals	60	28.9032		

The effect of "Space-Time Interactions" is not significant under 5% significance level. Since we know that, under stationarity, the covariance between any two measurements does not depend on their relative position, nonsignificance of this effect fails to reject that this spatial-temporal process satisfies stationarity. We also know that the "Directions" effect has no significant contribution to testing lack of axial symmetry in space. However, the effect of "Spatial Frequencies" is statistically significant. That strongly implies that there exists lack of axial symmetry in space, that is, $C(h_1, h_2; u) \neq C(-h_1, h_2; u)$.

Now we check whether lack of axial symmetry in space depends on the effect of "Directions" by performing the ANOVA technique for each directions; D5, and D6. From Table 3.6, we can see that, in the D6 direction, the effect of "Spatial Frequencies" is significant (p-value< 0.05). Thus, we conclude that, under certain direction lying in the two dimensional domain consisting of latitude and measuring time, lack of axial symmetry in space exists.

We check the lack of normality of residuals from the ANOVA technique in Table 3.6 by comparing with the quantiles from normal distribution with mean

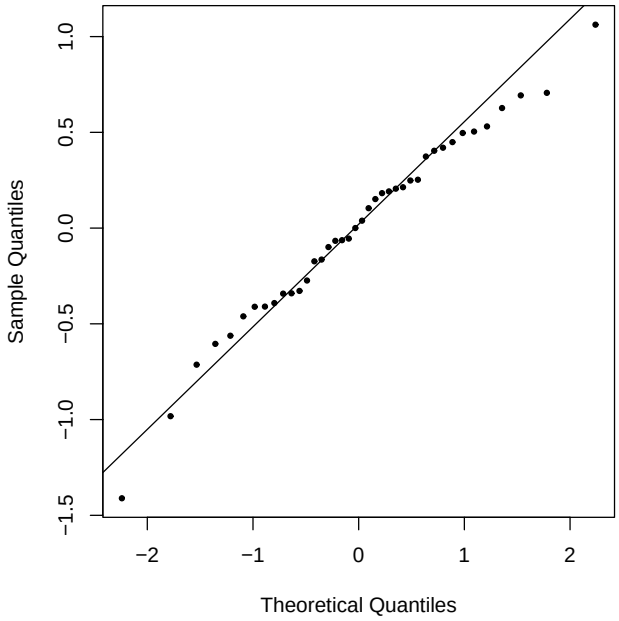

Figure 3.10: The QQplot of the residuals from the ANOVA technique in case of the D5 direction.

0 and variance 1. Figure 3.10 shows that the normality assumption seems to be reasonable. The p-value calculated from the Kolmogorov-Smirnov normality test is 0.89.

Based on the results from the tests for lack of axial symmetry in time and lack of axial symmety in space (see Table 3.5 and Table 3.6), we make the conclusion that the spatial-temporal process of $PM_{2.5}$ anomaly concentration is influenced by some external meteorological condition of which flow might be in E-W direction or W-E direction, and its spatial-temporal covariance has totally different behaviour in terms of the sign of first spatial distance.

3.6 Discussion

In this chapter, we introduced new concept of symmetry in spatial-temporal processes and proposed new formal tests for lack of axial symmetry in time and for lack of axial symmetry in space. We evaluated the performances of the tests by simulation study and applied to the real air-pollution data. The main advantages of these tests are that we can understand not only the existence of lack of symmetry but also the potential flow causing asymmetry.

As part of our further research, we are developing a formal test for lack of diagonal symmetry in space. This test could also be approached by the spectral representation that we have used in this study.

Table 3.5: Analysis of variance

Direction	Item	Degree of Freedom	Sum of Squares	F value	Pr(F)
D1	Locations	4	1.3933	25.8807	0.0000
	Frequencies	12	0.4283	2.6519	0.0118
	Residuals	36	0.4845		
D2	Locations	4	0.4026	4.0371	0.0083
	Frequencies	12	0.1201	0.4016	0.9536
	Residuals	36	0.8974		
D3	Locations	4	0.3358	2.5233	0.0578
	Frequencies	12	0.2819	0.7059	0.7354
	Residuals	36	1.1979		
D4	Locations	4	0.4522	5.3382	0.0018
	Frequencies	12	0.5186	2.0406	0.0491
	Residuals	36	0.7624		

Table 3.6: Analysis of variance

Direction	Item	Degree of Freedom	Sum of Squares	F value	Pr(F)
D5	Interactions	8	1.5599	0.3106	0.9555
	Frequencies	4	3.7268	1.4842	0.2336
	Residuals	28	17.5772		
D6	Interactions	8	3.3641	1.2229	0.3222
	Frequencies	4	4.6309	3.3668	0.0227
	Residuals	28	9.6284		

Chapter 4

Conclusion

In this study, we introduced new concepts of symmetry in spatial-temporal processes and proposed classes of asymmetric stationary spatial-temporal covariance models. Since these covariances are just Fourier transformations of the corresponding valid spectral density functions, they can easily be shown to be positive definite. Unlike a process with separable, even nonseparable covariance, an asymmetric spatial-temporal proecess is influenced by spatial-temporal dependencies, which are mainly controled by asymmetry parameters. This characteristic is very helpful to analyze the air-pollution data affected by some external metheological conditions, for instance, wind speed, wind direction, air pressure and so on.

The asymmetric covariance models can be extended to the spatial domain with $d > 2$ although our results presented in this study are based on the two dimensional spatial domain. For example, in case of spatial domain with longitude, latitude and altitude, the asymmetric covariance models are constructed in $\mathbb{R}^3 \times \mathbb{R}$. As part

of our further research, we are estimating the parameters by means of Bayesian approach taking into account uncertainties in the covariance models.

we also introduced new concept of symmetry in spatial-temporal processes and proposed new formal tests for lack of axial symmetry in time and for lack of axial symmetry in space. We evaluated the performances of the tests by simulation study and applied to the real air-pollution data. The main advantages of these tests are that we can understand not only the existence of lack of symmetry but also the potential flow causing asymmetry. As part of our further research, we are developing a formal test for lack of diagonal symmetry in space. This test could also be approached by the spectral representation that we have used in this study.

Chapter 5

Appendix

5.1 The derivation of the asymmetric stationary spatial-temporal covariance function

Suppose that the $(d+1)$ dimensional spectal density function is defined as

$$f_0(\boldsymbol{\omega};\tau) \equiv \gamma(\alpha^2\beta^2 + \beta^2\|\boldsymbol{\omega}\|^2 + \alpha^2\tau^2)^{-\nu},$$

γ, α and β are positive, and $\nu > \frac{d+1}{2}$. Then the corresponding covariance function can be derived like the following way:

$$\begin{aligned} C_0(\mathbf{h};u) &= \int_{\mathbb{R}}\int_{\mathbb{R}^d} f_0(\boldsymbol{\omega};\tau)\exp\{i\mathbf{h}'\boldsymbol{\omega} + iu\tau\}d\boldsymbol{\omega}\, d\tau \\ &= \gamma\int_{\mathbb{R}}\exp\{iu\tau\}\int_{\mathbb{R}^d}\left\{\alpha^2\left(\beta^2+\tau^2\right)+\beta^2\|\boldsymbol{\omega}\|^2\right\}^{-\nu}\exp\{i\mathbf{h}'\boldsymbol{\omega}\}d\boldsymbol{\omega}\, d\tau. \end{aligned}$$

By Stein (2005),

$$\int_{\mathbb{R}^d} \left\{\alpha^2\left(\beta^2+\tau^2\right)+\beta^2\|\boldsymbol{\omega}\|^2\right\}^{-\nu}\exp\{i\mathbf{h}'\boldsymbol{\omega}\}d\boldsymbol{\omega}$$
$$=\frac{\pi^{d/2}\beta^{-2\nu}}{2^{\nu-d/2-1}\Gamma(\nu)}\left\{\frac{\alpha}{\beta}\sqrt{\beta^2+\tau^2}\right\}^{-2\nu+d}\mathcal{M}_{\nu-d/2}\left(\frac{\alpha}{\beta}\sqrt{\beta^2+\tau^2}\|\mathbf{h}\|\right),$$

where $\mathcal{M}_\nu(r)=r^\nu\mathcal{K}_\nu(r)$. And, by Gradshteyn and Ryzhik (2000, pp.730, Eq.6.726 4),

$$\begin{aligned}\mathcal{L}_\nu(\mathbf{h};u) &\equiv \int_{\mathbb{R}}\left(\beta^2+\tau^2\right)^{-(\nu-d/2)/2}\mathcal{K}_{\nu-d/2}\left(\frac{\alpha}{\beta}\sqrt{\beta^2+\tau^2}\|\mathbf{h}\|\right)\exp\{iu\tau\}d\tau\\ &= 2\int_0^\infty\left(\beta^2+\tau^2\right)^{-(\nu-d/2)/2}\mathcal{K}_{\nu-d/2}\left(\frac{\alpha}{\beta}\sqrt{\beta^2+\tau^2}\|\mathbf{h}\|\right)\cos\{u\tau\}d\tau\\ &= \sqrt{2\pi}(\alpha\|\mathbf{h}\|)^{-\nu+d/2}\beta^{-\nu+d/2+1}\mathcal{M}_{\nu-\frac{d+1}{2}}\left(\beta\sqrt{\frac{\alpha^2}{\beta^2}\|\mathbf{h}\|^2+u^2}\right).\end{aligned}$$

Then we can obtain the closed form of the $(d+1)$ dimensional covariance function given by

$$\begin{aligned}C_0(\mathbf{h};u) &= \frac{\gamma\pi^{d/2}\|\mathbf{h}\|^{\nu-d/2}}{2^{\nu-d/2-1}\Gamma(\nu)}\alpha^{-\nu+d/2}\beta^{-\nu-d/2}\mathcal{L}_\nu(\mathbf{h};u)\\ &= \frac{\gamma\pi^{(d+1)/2}\alpha^{-2\nu+d}\beta^{-2\nu+1}}{2^{\nu-(d+1)/2-1}\Gamma(\nu)}\mathcal{M}_{\nu-\frac{d+1}{2}}\left(\beta\sqrt{\frac{\alpha^2}{\beta^2}\|\mathbf{h}\|^2+u^2}\right).\end{aligned}$$

5.2 The asymptotic normality of $\widehat{\phi}^*_{\mathbf{ab}}(\tau)$ in (3.18)

Fuentes (2005) provides the asymptotic normality and independence of the cross-spectral density function, $\widehat{f}_{\mathbf{ab}}(\tau)$ evaluated at different frequencies and locations. The approximate independence between $\widehat{f}_{\mathbf{a}_i\mathbf{b}_i}(\tau)$ and $\widehat{f}_{\mathbf{a}_j\mathbf{b}_j}(\lambda)$ is also obtained under either of the conditions, **C.1** and **C.2**. Based on the information from Fuentes (2005), we try to find the asymptotic distribution of $\widehat{\phi}^*_{\mathbf{ab}}(\tau)$ in (3.18).

Suppose that $\widehat{\phi}^{*}_{ik} \equiv \widehat{\phi}^{*}_{\mathbf{a}_i\mathbf{b}_i}(\tau_k)$, $\widehat{\boldsymbol{\Theta}} \equiv \left(\widehat{\phi}^{*}_{ik}, \widehat{\phi}^{*}_{jl}\right)'$, and $\widehat{\boldsymbol{\theta}} \equiv \left(\widehat{\phi}_{ik}, \widehat{R}_{ik}, \widehat{\phi}_{jl}, \widehat{R}_{ik}\right)'$, where $\widehat{\phi}_{ik}$ and $\widehat{R}_{ik}$ are the phase and the coherency at the i_{th} pair at the temporal frequency τ_k. Then, by Taylor-series expansion,

$$\widehat{\boldsymbol{\Theta}} = \boldsymbol{\Theta} + \frac{\partial \widehat{\boldsymbol{\Theta}}}{\partial \boldsymbol{\theta}} \left(\widehat{\boldsymbol{\theta}} - \boldsymbol{\theta}\right) + \mathbf{o}_p(B_T^{-1}T^{-1}),$$

where $\boldsymbol{\Theta} = \left(\phi^{*}_{ik}, \phi^{*}_{jl}\right)'$, and $\boldsymbol{\theta} = (\phi_{ik}, R_{ik}, \phi_{jl}, R_{ik})'$. Under the null hypothesis that $\phi_{ik} = 0$ and $\phi_{jl} = 0$, we can reexpress the previous equation as

$$\widehat{\boldsymbol{\Theta}} = \boldsymbol{\Theta}_0 + \frac{\partial \widehat{\boldsymbol{\Theta}}}{\partial \boldsymbol{\theta}_0} \left(\widehat{\boldsymbol{\theta}} - \boldsymbol{\theta}_0\right) + \mathbf{o}_p(B_T^{-1}T^{-1}),$$

where $\boldsymbol{\Theta}_0 = (0, 0)'$, $\boldsymbol{\theta}_0 = (0, R_{ik}, 0, R_{jl})'$, and

$$\frac{\partial \widehat{\boldsymbol{\Theta}}}{\partial \boldsymbol{\theta}_0} = \begin{pmatrix} \frac{1}{\left[|R_{ik}|^{-2}-1\right]^{1/2}} & 0 & 0 & 0 \\ 0 & 0 & \frac{1}{\left[|R_{jl}|^{-2}-1\right]^{1/2}} & 0 \end{pmatrix}.$$

Under the assumptions **A.1** through **A.3**, we asymptotically obtain the mean and the variance $\boldsymbol{\Sigma}_{\boldsymbol{\Theta}}$, which is denoted by

$$\begin{aligned} \boldsymbol{\Sigma}_{\boldsymbol{\Theta}} &= (B_T T) \left(\frac{\partial \widehat{\boldsymbol{\Theta}}}{\partial \boldsymbol{\theta}_0}\right) \boldsymbol{\Sigma}_{\boldsymbol{\theta}} \left(\frac{\partial \widehat{\boldsymbol{\Theta}}}{\partial \boldsymbol{\theta}_0}\right)' \\ &= \begin{pmatrix} \frac{B_T T \mathrm{Var}\left(\widehat{\phi}_{ik}\right)}{\left[|R_{ik}|^{-2}-1\right]} & \frac{B_T T \mathrm{cov}\left(\widehat{\phi}_{ik}, \widehat{\phi}_{jl}\right)}{\left[|R_{ik}|^{-2}-1\right]^{1/2}\left[|R_{jl}|^{-2}-1\right]^{1/2}} \\ \frac{B_T T \mathrm{cov}\left(\widehat{\phi}_{jl}, \widehat{\phi}_{ik}\right)}{\left[|R_{ik}|^{-2}-1\right]^{1/2}\left[|R_{jl}|^{-2}-1\right]^{1/2}} & \frac{B_T T \mathrm{Var}\left(\widehat{\phi}_{jl}\right)}{\left[|R_{jl}|^{-2}-1\right]} \end{pmatrix}, \end{aligned}$$

where $\boldsymbol{\Sigma}_{\boldsymbol{\theta}} = E\left[\left(\widehat{\boldsymbol{\theta}} - \boldsymbol{\theta}_0\right)\left(\widehat{\boldsymbol{\theta}} - \boldsymbol{\theta}_0\right)'\right]$. If either of the conditions **C.1** and **C.2** is satisfied, then $\widehat{\phi}_{\mathbf{a}_i\mathbf{b}_i}(\tau_k)$ is approximately independent of $\widehat{\phi}_{\mathbf{a}_j\mathbf{b}_j}(\tau_l)$ if and only if $\widehat{f}_{\mathbf{a}_i\mathbf{b}_i}(\tau_k)$ is apprximately independent of $\widehat{f}_{\mathbf{a}_j\mathbf{b}_j}(\tau_l)$. Therefore, we finally compute

the following asymptotic variance:

$$\boldsymbol{\Sigma}_{\boldsymbol{\Theta}} = \begin{pmatrix} \pi \left(\int_{\mathbb{R}} W^2(\alpha)\, d\alpha \right) [1 - \eta\{2\tau_k\}] & 0 \\ 0 & \pi \left(\int_{\mathbb{R}} W^2(\alpha)\, d\alpha \right) [1 - \eta\{2\tau_l\}] \end{pmatrix}.$$

Bibliography

[1] Noel A. Cressie and Hsin-Cheng Huang. Classes of nonseparable, spatio-temporal stationary covariance functions. *Journal of the American Statistical Association,* 94:1330-1340, 1999.

[2] T. Gneiting. Nonseparable, stationary covariance functions for space-time data. *Journal of the American Statistical Association,* 97:590-600, 2002.

[3] M. Fuentes, L. Chen, J. Davis, and G. Lackmann. Modeling and predicting complex space-time structures and patterns of coastal wind fields. *Environmetrics,* 16:449-464, 2005.

[4] L. Scaccia and R. J. Martin. Testing axial symmetry in separability in lattice processes. *Journal of Statistical Planning and Inference,* 131:19-39, 2005.

[5] D. Zimmerman. Another look at anisotropy in geostatistics. *Mathematical Geology,* 25:453-471, 1993.

[6] I. Rodriguez-Iturbe and J. M. Mejia. The design of rainfall newtorks in time and space. *Water Resources Research,* 10:713-729, 1974.

[7] R. H. Jones and Y. Zhang. Models for continuous stationary space-time processes. in *Modelling Longitudinal and Spatially correlated Data,* (Lecture Notes in Statistics 122), eds. T. G. Grogorie, D. R. Brillinger, P. J. Diggle, E. Russek-Cohen, W. G. Warren, and R. D. Wolfinger, pages 289-298. Springer, 1997.

[8] D. E. Myers and A. G. Journel. Variograms with zonal anisotropies and noninvertible kriging systems. *Mathematical Geology,* 22:779-785, 1990.

[9] S. Rouhani and D. E. Myers. Problems in space-time kriging of geohydrological

data. *Mathematical Geology,* 22:611-623, 1990.

[10] N. Lu and D. L. Zimmerman. Testing for directional symmetry in spatial dependence using the periodogram. *Journal of Statistical Planning and Inference,* 129:369-385, 2005.

[11] M. L. Stein. Space-time covariance functions. *Journal of the American Statistical Association,* 100:310-321, 2005.

[12] I. S. Gradshteyn and I. M. Ryzhik. *Table of Integrals, Series, and Products (Sixth Edition).* Academic Press, 2000.

[13] J. V. Zidek. Interpolating air pollution for health impact assessment. In *Statistics for Environment 3: Pollution Assessment and Control,* eds. V. Barnett, and K. Feridun Turkman, New York: Wiley, p251-268, 1997.

[14] B. M. Golam Kibria, L. Sun, J. V. Zidek, and N. D. Le. Bayesian spatial prediction of random space-time fields with application to mapping $PM_{2.5}$ exposure. *Journal of the American Statistical Association,* 97:112-124, 2002.

[15] N. Cressie. *Statistics for spatial data.* John Wiley & Sons, 1993.

[16] M. Shitan and P. Brockwell. An asymptotic test for separability of a spatial autoregressive model. *Communications in Statistics-Theory and Methods,* 24:2027-2040, 1995.

[17] J. H. Guo and L. Billard. Some inference results for causual autoregressive processes on a plane. *Journal of Time Series Analysis,* 19:681-691, 1998.

[18] M. Mitchell. Testing separability of covariances for space-time processes. Ph.D. Thesis at the Statistics Department, North Carolina State University, 2002.

[19] M. Mitchell, M. G. Genton, and M. Gumpertz. A likelihood ratio test for separability of covariances, manuscript under review, (http://www4.ncsu.edu:8030/mwmitch2/Biom.pdf), 2002.

[20] M. Fuentes. Testing for separability of spatial-temporal covariance functions. *Journal of Statistical Planning and Inference,* 136:447-466, 2006.

[21] A. M. Yaglom. *Correlation theory of stationary and related random functions I.* Springer Verlag, 1987.